

UNIVERSITÀ DEGLI STUDI DI NAPOLI "FEDERICO II"

FACOLTÀ DI INGEGNERIA



Dottorato di ricerca in Ingegneria dei Materiali e delle Strutture
XIV ciclo

STRUCTURE AND DYNAMICS OF MODEL POLYMER NANOCOMPOSITES

Relatore

CH. MO PROF.

Domenico Acierno

Candidato

Ing. Guglielmo Capuano

Coordinatore

CH.MO PROF.

Domenico Acierno

Triennio 2008/2011

Contents

Chapter 1. Polymer Nanocomposites

1.1 Introduction.....	5
1.2 Structural probes of polymer nanocomposites.....	8
1.2.1 Microscopic techniques.....	9
1.2.2 Radiation scattering techniques.....	10
1.2.3 Rheology.....	11

Chapter 2. Dynamics of Nanoparticles in Polymer Melts

2.1 Introduction.....	15
2.2 Viscoelasticity and structure of PNCs.....	21
2.3 Brownian motion of nanoparticles in polymer melts – Gelation and ageing.....	22
2.3.1 Preliminary considerations.....	22
2.3.2 Materials and sample preparation.....	23
2.3.3 Characterization.....	26
2.3.4 Effect of the filler mobility on the linear viscoelasticity.....	27
2.4 Linear viscoelasticity of PNCs.....	35
2.4.1 Weakly attractive particles suspended in Newtonian fluids – A two-phase model.....	35
2.4.2 Weakly attractive nanoparticles suspended in non-Newtonian mediums – Recovering the two-phase Model.....	38
2.4.3 Refining the two-phase model – Role of the hydrodynamic effects.....	42
2.5 Strength and reversibility of the filler network in PP/Al ₂ O ₃ PNCs.....	46
2.6 Conclusions.....	52

Chapter 3. Scaling the Melt-Elasticity of Interacting Polymer Nanocomposites. *Universal Features of PEO/SiO₂ Mixtures at Different Filler Content and State of Dispersion*

3.1 Introduction.....	55
3.2 Experimental.....	58
3.2.1 Raw materials.....	58
3.2.2 Nanocomposites preparation.....	59
3.2.3 Characterization	60
3.3 Results and Discussion.....	62
3.3.1 MC samples: structure and linear viscoelasticity.....	62
3.3.2 Linear viscoelasticity: Two-phase model.....	66
3.3.3 <i>Freeze-Dried</i> samples: Role of the state of filler dispersion on the linear viscoelasticity.....	69
3.3.4 Elasticity and structure of the PEO/SiO ₂ composites above ϕ_c	73
3.4 Conclusions.....	76

Chapter 4. Role of Polymer–Particle interactions on the Dynamics of Polymer Nanocomposites *Glass Transition and Reinforcement Mechanism in PMA/SiO₂ Mixtures*

4.1 Introduction.....	78
4.2 Experimental.....	82
4.2.1 Raw materials.....	82
4.2.2 Nanocomposites preparation.....	83
4.2.3 Characterization.....	84
4.3 Results and discussion.....	85
4.3.1 Structure and dynamics PMA/Colloidal Silica Mixtures.....	85
4.3.2 Dispersion morphology.....	94
4.4 Origin of the dynamic behavior.....	95

4.4.1 Free Volume and Polymer Entanglement Density....	96
4.4.2 The “Filler” Effect.....	97
4.4.3 Factors of Influence on PMMA Matrix Properties....	98
4.4.4 Role of Transient Interactions at Interfacial Contact.....	100
References.....	102

Chapter 1

Polymer nanocomposites

1.1 Introduction

The use of organic or inorganic filler has become ubiquitous in polymeric systems. Polymer composites are manufactured commercially for many diverse applications such as sporting goods, aerospace components, automobiles, etc. In the last 20 years, there has been a strong emphasis on the development of polymeric nanocomposites, where at least one of the dimensions of the filler material is of the order of a nanometer. The final product does not have to be in nanoscale, but can be micro- or macroscopic in size. This surge in the field of nanotechnology has been greatly facilitated by the advent of scanning tunneling microscopy and scanning probe microscopy in the early 1980s. With these powerful tools, scientists are able to see the nature of the surface structure with atomic resolution. Simultaneously, the rapid growth of computer

technology has made it easier to characterize and predict the properties at the nanoscale via modeling and simulation.

In general, the unique combination of the nanomaterial's characteristics, such as size, mechanical properties, and low concentrations necessary to effect change in a polymer matrix, coupled with the advanced characterization and simulation techniques now available, have generated much interest in the field of nanocomposites. In addition, many polymer nanocomposites can be fabricated and processed in ways similar to that of conventional polymer composites, making them particularly attractive from a manufacturing point of view.

The transition from microparticles to nanoparticles yields dramatic changes in physical properties. Nanoscale materials have a large surface area for a given volume. Since many important chemical and physical interactions are governed by surfaces and surface properties, a nanostructured material can have substantially different properties from a larger-dimensional material of the same composition. In the case of particles and fibers, the surface area per unit volume is inversely proportional to the material's diameter, thus, the smaller the diameter, the greater the surface area per unit volume. A change in particle diameter, layer thickness, or fibrous material diameter from the micrometer to nanometer range, will affect the surface area-to-volume ratio by three orders of magnitude. Typical nanomaterials currently under investigation include nanoparticles, nanotubes, nanofibers,

fullerenes, and nanowires. In general, these materials are classified by their geometries; broadly the three classes are particle, layered, and fibrous materials. Carbon black, silica nanoparticle, polyhedral oligomeric silsesquioxanes (POSS) can be classified as nanoparticle reinforcing agents while nanofibers and carbon nanotubes are examples of fibrous materials. When the filler has a nanometer thickness and a high aspect ratio (30–1000) plate-like structure, it is classified as a layered nanomaterial (such as an organosilicate).

In general, nanomaterials provide reinforcing efficiency because of their high aspect ratios. The properties of a nanocomposite are greatly influenced by the size scale of its component phases and the degree of mixing between the two phases. Depending on the nature of the components used (layered silicate or nanofiber, cation exchange capacity, and polymer matrix) and the method of preparation, significant differences in composite properties may be obtained. Analogously, in fibrous or particle-reinforced polymer nanocomposites (PNCs), dispersion of the nanoparticle and adhesion at the particle–matrix interface play crucial roles in determining the mechanical properties of the nanocomposite. Without proper dispersion, the nanomaterial will not offer improved mechanical properties over that of

conventional composites, in fact, a poorly dispersed nanomaterial may degrade the mechanical properties. Additionally, optimizing the

interfacial bond between the particle and the matrix, one can tailor the properties of the overall composite, similar to what is done in macrocomposites. For example, good adhesion at the interface will improve properties such as interlaminar shear strength, delamination resistance, fatigue, and corrosion resistance.

1.2 Structural probes of polymer nanocomposites

Quantitative characterization of the dispersion and the orientation states of nanoparticles and the polymer matrix are critical for developing fundamental structure-properties correlations. However, such efforts are often difficult, partly because of the range of the length scales associated with such materials, but also owing to the polydispersity and heterogeneity of the nanoparticles. Typically, structural characterization tools include force, optical and electron microscopy; X-ray, neutron and light scattering; chemical spectroscopic methods; electrical and dielectrical characterization and mechanical spectroscopy. Depending on the details of the nanoparticles and the polymer matrix, each of these methods can provide unique information on the dispersion state and polymer and nanoparticle arrangements over size scales ranging from nanometers to millimeters. Also the combined use of these techniques can provide detailed information on the hierarchical morphology in nanocomposites. For thermal characterization and to study the cure behavior (typically for thermoset

resin systems) of PNCs, the commonly used techniques are differential scanning calorimeter (DSC), thermogravimetric analysis (TGA), thermomechanical analysis (TMA), Fourier-transform infrared (FTIR), dynamic modulus analysis (DMA), rheometer, etc.

Microscopic and radiation scattering characterization tools are crucial to comprehend the basic physical and chemical properties of PNCs. For structural applications, it facilitates the study of emerging materials by giving information on some intrinsic properties. Various techniques for characterization have been used extensively in polymer nanocomposite research. The commonly used powerful techniques are wide-angle X-ray diffraction (WAXD), small-angle X-ray scattering (SAXS), scanning electron microscopy (SEM), and transmission electron microscopy (TEM).

1.2.1 Microscopic techniques

The SEM provides images of surface features associated with a sample. However, there are two other microscopies, scanning probe microscopy (SPM) and scanning tunneling microscopy (STM), which are indispensable in nanotube research. The SPM uses the interaction between a sharp tip and a surface to obtain an image. In STM, a sharp conducting tip is held sufficiently close to a surface (typically about 0.5 nm), such that electrons can 'tunnel' across the gap. This method provides surface structural and electronic information at atomic level.

The invention of the STM inspired the development of other 'scanning probe' microscopes, such as the atomic force microscope (AFM). The AFM uses a sharp tip to scan across the sample. Raman spectroscopy has also proved a useful probe of carbon-based material properties. TEM allows a qualitative understanding of the internal structure, spatial distribution of the various phases, and views of the defective structure through direct visualization, in some cases of individual atoms.

1.2.2 Radiation scattering techniques

Due to the easiness and availability, WAXD is the most commonly used to probe the nanocomposite structure and occasionally to study the kinetics of the polymer melt intercalation. In layered silicate nanocomposite systems, a fully exfoliated system is characterized by the absence of intensity peaks in WAXD pattern e.g., in the range $1.5^\circ \leq 2\theta \leq 10^\circ$, which corresponds to a d-spacing of at least 6 nm. Therefore, a WAXD pattern concerning the mechanism of nanocomposite formation and their structure are tentative issues for making any conclusion. Therefore, TEM complements WAXD data [26]. Small-angle X-ray scattering (SAXS) is typically used to observe structures on the order of 10 \AA or larger, in the range of 0° or 0.5° - 5° . The TEM, AFM, and SEM, are also required to characterize nanoparticle, carbon nanofiber dispersion, or distribution. However, X-ray

diffraction has found relatively limited success in CNT research. Both TEM and WAXD are essential tools for evaluating nanocomposite structure. However, TEM is time-intensive, and only gives qualitative information on the sample as a whole, while low-angle peaks in WAXD allow quantification of changes in layer spacing. Typically, when layer spacing exceeds 6–7 nm in intercalated nanocomposites or when the layers become relatively disordered in exfoliated nanocomposites, associated WAXD features weaken to the point of not being useful. However, simultaneous small angle X-ray scattering (SAXS) and WAXD studies yielded quantitative characterization of nanostructure and crystallite structure in N6 based nanocomposites. Very recently, Bafna et al. developed a technique to determine the three-dimensional (3D) orientation of various hierarchical organic and inorganic structures in a PLS nanocomposite. They studied the effect of compatibilizer concentration on the orientation of various structures in PLS nanocomposites using 2D SAXS and 2D WAXD in three sample/camera orientations.

1.2.3 Rheology

Rheology is a science that studies the deformation of materials as a result of an applied stress. It is useful in characterizing soft condensed matter including complex and structured fluids, such as polymer melts and polymer nanocomposites. This importance in characterizing

colloidal systems arises from the fact that information on their mesostructures in equilibrium and under flow conditions can be obtained by using appropriate rheological techniques¹. Moreover, valuable knowledge on processing of these materials can be also obtained from these measurements. Rheological measurements can be performed under steady or dynamic shear mode and, depending upon the response of the fluid, the microstructure can be probed.

Steady Shear

In steady shear rheology, a sample is deformed by applying a constant shear rate. After an adequate period of time, the shear stress (τ) reaches steady state and a material function, called the apparent viscosity (η), can be determined by taking the ratio between stress and shear rate:

The behavior of η as a function of $\dot{\gamma}$ (or flow curve) is used to classify the flow behavior of fluids. If the apparent viscosity does not depend on the applied shear rate, the fluid is known as Newtonian. Fluids that observe a viscosity increase with shear rate are named shear thickening and those with a decrease in viscosity as a function of shear rate are shear thinning. Some fluids flow after exceeding a certain stress value; this stress is known as the yield stress and it indicates the susceptibility of the microstructure to breakdown under applied forces.

Dynamic Shear

Oscillatory shear or dynamic mechanical spectroscopy experiments impose small amplitude oscillatory shearing to the sample. For example, if a sinusoidal strain (γ) is applied:

$$\gamma = \gamma_0 \sin(\omega t)$$

where γ_0 is the strain amplitude and ω the frequency of oscillation. The resulting

stress τ varies sinusoidally with time and is :

$$\tau = \tau_0 \sin(\omega t + \delta) = G'(\omega) \sin(\omega t) + G''(\omega) \cos(\omega t)$$

τ is not necessarily in phase with the applied strain (δ is the phase angle), and if γ_0 is small enough (usually $\ll 1$), the stress is represented according to eqn. The regime in which this equation is valid is known to as the linear viscoelastic regime, $G'(\omega)$ and $G''(\omega)$ are the storage and loss modulus, respectively. The storage modulus is in phase with the strain and is commonly associated with the elastic energy of the material, whereas the loss modulus is in phase with the strain rate and represents the viscous dissipation of that energy. The ratio G''/G' is known as the loss tangent ($\tan\delta$) and is higher than unity for liquid-like materials, and smaller than unity for materials that behave like solids.

The importance of this type of measurements arises from the fact that at low strain values the "at rest" microstructure can be probed since it is not disrupted by shearing as in steady shear flow experiments. This is very useful in colloidal systems because the state of aggregation can be associated with the particular rheological response within the linear

viscoelastic regime obtained from the dynamic mechanical spectrum of the material, $G'(\omega)$ and $G''(\omega)$.

Chapter 2

Dynamics of Nanoparticles in Polymer Melts

2.1 Introduction

Adding solid particles to polymeric materials is a common way to reduce the costs and to achieve desired mechanical, electrical, thermal and transport properties. This makes polymers potential substitutes for more expensive non-polymeric materials. The advantages of filled polymers are normally offset by the increased complexity in their rheological behaviour. Usually, a compromise has to be made between the benefits ensured by the filler, the increased difficulties in melt processing, the problems in achieving a uniform dispersion of the solid particulate, and the economics of the process due to the additional compounding step [Shenoy, 1999]. Filled polymers can be depicted as a suspension of particles and particle aggregates dispersed in the polymer matrix. Interactions between individual particles or aggregates and the matrix, as well as between particles, hinder the deformability of the polymer matrix modifying both its solid- and melt-state behaviour. In polymer-based microcomposites, these effects only become significant

at relatively high filler contents, i.e. when the filler particles are sufficiently close to each other to form a network that spans large sections of the polymer matrix. Over the last fifteen years, the same reinforcing and thixotropic effects have been observed with the use of very small amounts of inorganic nanoparticles, which has resulted in extensive research in the field of polymer-based nanocomposites (PNCs) [Usuki et al., 1993; Kojima et al., 1993]. In order to fully understand the exceptional properties of PNCs, it is necessary to take into account the morphological and structural implications stemming from the nanometric sizes of the filler. With respect to traditional microcomposites, nanocomposites show very high specific interface area, typically of order of $\sim 10^2 \text{ m}^2 \text{ g}^{-1}$. The properties of the matrix are significantly affected in the vicinity of the reinforcement, varying continuously from the interface towards the bulk polymer. As a consequence, the large amount of reinforcement surface area means that a relatively small amount of nanoscale reinforcement can have remarkable effects on the macroscale properties of the composite material.

A noticeable consequence of the nanometric dimensions of the filler is the extremely high numerical density of particles, or alternatively the very small inter-particles distances. If N monodisperse spherical particles with radius r are randomly distributed in a volume V , the distance between the centres of the particles can be approximated to

$h=(V/N)^{1/3}$. Introducing the particle volume fraction $\Phi=Nv/V$, where $v=4\pi r^3/3$ is the volume of the single particle, the wall-to-wall distance between contiguous particles is:

$$h = \left[\sqrt[3]{\frac{4\pi}{3\Phi}} - 2 \right] r \quad (1)$$

Once fixed the filler content, h linearly scales with r . In addition, we observe that, for diluted systems ($\Phi < 0.1$) such those we are interested in, Eq. 1 gives $h \sim 2r$. This means that, if the filler particles are well dispersed within the host polymer, nanometric inter-particles distances are expected for nanocomposites. In such systems a large fraction of polymer is in contact with the filler. At the most, if the particle radius is of the same order as the mean radius of gyration of host polymer chains, R_g , each single chain potentially interacts with more than one nanoparticle, and there is no bulk polymer [Jancar&Recman, 2010]. When these length scales converge, two scenarios are possible: if a good affinity exists between the polymer and the filler, then a polymer-mediated transient network between the particles set up [Ozmusul et al., 2005; Saint-Michel et al., 2003; Zhang & Archer, 2002]; on the other hand, if the polymer-filler interactions are weak, the nanoparticles aggregate forming flocs, which eventually assemble into a space-spanning filler network [Filippone et al. 2009; Inoubli et al., 2006; Ren et

al., 2000]. In both cases, the presence of a three-dimensional mesostructure has a profound effect on the composite rheology.

The formation of the network, either polymer-mediated or formed by bare nanoparticles, originates from local rearrangements of the filler occurring in the melt during flow or at rest. Nanoparticles, in fact, are subjected to relevant Brownian motion even in highly viscous mediums such as polymer melts. To get an idea about the relevance of such a phenomenon, we estimate the self-diffusion time of a spherical particle of radius r , τ_s , that is the time required for the particle to move over a length equal to its radius [Russel et al., 1989]:

$$\tau_s = \frac{6\pi\eta_s r^3}{k_B T} \quad (2)$$

Here η_s is the viscosity of the suspending medium, k_B is the Boltzmann's constant and T is the temperature. For a simple low viscosity ($\eta_s \sim 10^{-2}$ Pa*s) Newtonian liquid at room temperature, Eq. 2 gives the well-known result that particles of a few microns in size experience appreciable Brownian motions. Setting $T=400^\circ\text{K}$ and $\eta_s \sim 10^3$ Pa*s as typical values for polymer melts, we obtain the noteworthy result that particles of a few tens of nanometers display Brownian motions on timescales of order of a $10^1 \div 10^2$ seconds. Such time scales are typically accessed in many industrial manufacturing processes, as well as during

rheological experiments. The result is that, unlike polymer microcomposites, PNCs can be depicted as “living systems”, in which the particles are free to move and rearrange in the melt, both in flow and even at rest, towards more favourable thermodynamic states. In this sense, PNCs are reminiscent of colloidal suspensions. Therefore, these simple systems can be considered as the natural starting point to understand the much more complex rheological behaviour of PNCs.

The simplest case of colloidal dispersion is represented by a suspension of hard spheres. The inter-particles interaction is zero at all separations and infinitely repulsive at contact. When coupled with thermal fluctuations, this kind of interaction results in a wide variety of possible structures. The suspension may behave like a gas, a liquid, a crystal or a glass depending on the particle volume fraction Φ [Pusey & van Meegen, 1986]. When interactions become relevant, this phase behaviour is dictated by a subtle interplay between the volume fraction Φ and the interaction energy, U . In this chapter we will mainly deal with weakly attractive colloidal dispersions, which are reminiscent of a large number of PNCs in which Van der Waals forces between nanoparticles and aggregates are of major importance. In such systems, aggregation results in disordered clusters of particles. These mesostructures may or may not span the whole sample volume depending on the magnitude of Φ and U [Prasad, 2003]. The rheological behaviour of weakly interacting colloidal dispersions can be rationalized

with a simple two-phase model that combines the elasticity of the disordered particle network and the Newtonian viscosity of the suspending liquid [Cipelletti et al., 2000; Trappe & Weitz, 2000; Trappe et al., 2001]. Despite the complexities stemming from the intrinsic non-Newtonian feature of polymer matrices, in this chapter we show that a similar approach can be successfully applied to a series of model PNCs with weak polymer-filler interaction. We emphasize that many PNCs of technological interest fall in this category. The two-phase model is validated through the building of a master curve of the elastic modulus of samples at different composition. A refinement of the model is also presented, which accounts for hydrodynamic effects. In the next chapter we will extend the model to interacting systems. The dynamics of de-structuring and reforming of the filler network are studied by analysing the effects of large amplitude deformations. Besides simplifying the viscoelastic analysis of complex systems such as PNCs, the proposed approach can be extended to a wide variety of complex fluids where the elasticity of the components can be superimposed. In particular, the elastic modulus has been recently suggested to follow a universal behaviour with volume fraction also in case of interacting systems in which polymer bridging mechanisms exist [Surve et al., 2006]. This suggests a possible general feature for the proposed approach.

2.2 Viscoelasticity and structure of PNCs

We start our analysis dealing with the implications of Brownian motion in simple model systems based on polymer melts filled with small amounts of different kinds of spherical particles. Specifically, we discuss the effect of particle size and matrix viscosity on the ability of the filler to aggregate and eventually assemble in a three-dimensional network. Then, a two-phase model previously proposed for weakly attractive particles suspended in a Newtonian medium is presented [Trappe & Weitz, 2000]. The physical picture of an elastic particle network interspersed in a background fluid qualitatively accounts for the viscoelastic behaviour of the suspension. Afterwards, the relations between structure and viscoelasticity of two model PNCs is described in the framework of the two-phase model. A refinement of the model is therefore presented, which accounts for hydrodynamic effects successfully capturing the frequency dependent viscoelastic behaviour of simple PNCs. Finally, the dynamics of de-structuring and reforming of the filler network are studied by analysing the effects of large amplitude deformations.

2.3 Brownian motion of nanoparticles in polymer melts – Gelation and ageing

2.3.1 Preliminary considerations

Untreated inorganic particles are difficult to disperse in polymer matrices due to the typically poor polymer-filler affinity. Such incompatibility clearly emerges in the case of PNCs, where the specific surface of the particles is very high. The hydrodynamic forces developed during intense melt mixing processes breakup the large aggregates down to clusters of few tens of particles [Baird & Collias, 1998]. Above the melting or glass transition temperature of the polymer matrix, however, these aggregates may reassemble into bigger structures because of the inter-particles attraction forces. Since the refractive indexes of polymers and inorganic fillers are typically very different, Van der Waals forces becomes of major importance leading to formation of aggregates and particle gels. The two most simple experimental techniques to follow the rearrangements of the filler in the melt are: (i) direct visualization of the particles through electron microscopy performed on solid samples; (ii) monitoring of rheological parameters sensitive to the material internal structure. Both these techniques have been applied to several model PNC systems constituted by

polymermatrices filled with different kinds of inorganic nanoparticles with spherical symmetry. The rationale for selecting such model systems originates from the intrinsic high complexity of other technologically relevant PNCs. The properties of such systems, often based on layered or tubular nanoparticles, are too sensitive to the state of dispersion of the filler and the wide variety of the possible nanostructures achievable during processing. The materials, the compounding procedures and the experimental details about the characterization of the composites are described in detail in the following paragraphs. Many of the results have been taken from papers previously published by our group, wherein further experimental details can be found [Acierno et al., 2007a, 2007b; Romeo et al., 2008; Filippone et al., 2010; Romeo et al., 2009].

2.3.2 Materials and sample preparation

Nano- and microcomposites were prepared using two different polymeric matrices. The first one is polypropylene (PP Moplen HP563N by Basell; weight average molecular weight $M_w=245$ KDa; zero shear viscosity $\eta_0=1.9 \cdot 10^3$ Pa*s at 190°C; terminal relaxation time $\tau_t \approx 0.4$ s) with glass transition temperature $T_g=6^\circ\text{C}$ and melting temperature $T_m=169^\circ\text{C}$. The second polymer matrix is atactic polystyrene (PS, kindly supplied by Polimeri Europa). In particular, we used two PS matrices at different molecular weight, coded as PS-low ($M_w=125$ KDa;

$\eta_0=1.7 \cdot 10^3 \text{ Pa} \cdot \text{s}$ at 200°C ; $\tau_f \approx 0.1 \text{ s}$) and PS-high ($M_w=268 \text{ KDa}$; $\eta_0=2.1 \cdot 10^4 \text{ Pa} \cdot \text{s}$ at 200°C ; $\tau_f \approx 100 \text{ s}$), both having glass transition temperatures $T_g=100^\circ\text{C}$.

Three kinds of nanoparticles were used as fillers: titanium dioxide (TiO_2 by Sigma Aldrich; density $\rho=3.9 \text{ g/mL}$; surface area $\sim 190\div 290 \text{ m}^2/\text{g}$; average primary particles diameter $d=15 \text{ nm}$) and alumina nanospheres (Al_2O_3 by Sigma Aldrich; $\rho=4.00 \text{ g/mL}$; surface area: $35\text{--}43 \text{ m}^2/\text{g}$; $d \approx 40 \text{ nm}$) were used to prepare PP/ TiO_2 and PP/ Al_2O_3 nanocomposites with filler volume fractions up to $\Phi=0.064$; fumed silica (SiO_2 by Degussa; $\rho=2.2 \text{ g/mL}$; surface area $\sim 135\text{--}165 \text{ m}^2/\text{g}$; $d=14 \text{ nm}$) was mixed with the two PS matrices up to $\Phi=0.041$. PP/ TiO_2 microcomposites were also prepared by using titanium dioxide microparticles (TiO_2 by Sigma Aldrich; $\rho=3.9 \text{ g/mL}$; surface area $\sim 0.14\text{--}0.04 \text{ m}^2/\text{g}$; $d \approx 4 \mu\text{m}$).

Nano- and microcomposites were prepared by melt compounding the constituents using a co-rotating extruder (Minilab Microcompounder, ThermoHaake) equipped with a capillary die (diameter 2 mm). The extrusions were carried out at 190°C . The screw speed was set to $\sim 100 \text{ rpm}$, corresponding to an average shear rate of order of 50 s^{-1} inside the extrusion chamber. A feedback chamber allowed an accurate control of the residence time, which was set to 250 s for all the samples. The polymer and the filler were previously dried under vacuum for sixteen hours at 70°C . The neat polymers used as reference materials were

extruded in the same conditions to allow for an accurate comparison with the filled samples.

2.3.3 Characterization

The morphology of the composites was examined by transmission electron microscopy (TEM mod. EM 208, Philips). The observations were performed on slices with thickness ~150 nm, which were randomly cut from the extruded pellets using a diamond knife at room temperature. Rheological tests were carried out by means of either a strain-controlled rotational rheometer (ARES L.S, Rheometric Scientific) or a stress-controlled rotational rheometer (ARG2, TA Instruments). The tests were carried out using parallel plates with diameter of 25 mm for the nanocomposites, while plates of 50 mm were used for the neat polymers because of their low viscosity. All measurements were performed in an atmosphere of dry nitrogen. The testing temperature was $T=190^{\circ}\text{C}$ for the PP/TiO₂ samples and $T=200^{\circ}\text{C}$ for the PS/SiO₂ samples. The viscoelastic moduli display a range of strain-independence, i.e. a range of linear viscoelasticity, which depends on the filler content. In order to determine the limits of the linear viscoelastic regime, oscillatory strain scans were performed on each sample at a fixed frequency of 0.063 rad s^{-1} . Low-frequency ($\omega=0.063\text{ rad s}^{-1}$) time-sweep experiments were performed to study the evolution of the linear viscoelastic properties during time. The frequency-dependent elastic (G') and viscous (G'') moduli of the samples were measured by oscillatory shear scans in the linear regime. To account for the marked

sensitivity of the rheological response on filler content, we evaluated the effective amount of filler of each sample used for the rheological experiments through thermogravimetric analyses (TGA). The filler volume fraction Φ was estimated as:

$$\Phi = \frac{c\rho_p}{\rho_f + c(\rho_p - \rho_f)} \quad (3)$$

where c is filler weight fraction as deduced from TGA and ρ_p and ρ_f are the densities of polymer and filler, respectively.

2.3.4 Effect of the filler mobility on the linear viscoelasticity

The internal structure of the as extruded sample PP/TiO₂ at $\Phi=0.038$ is shown in the TEM micrograph of Figure 1.a. Well distributed nanoparticle aggregates of a few hundreds of nanometers are suspended in the polymer matrix. The magnification of one of these aggregates is reported in Figure 1.b. A few hundreds of individual TiO₂ nanoparticles are closely packed to form dense clusters with irregular shape.

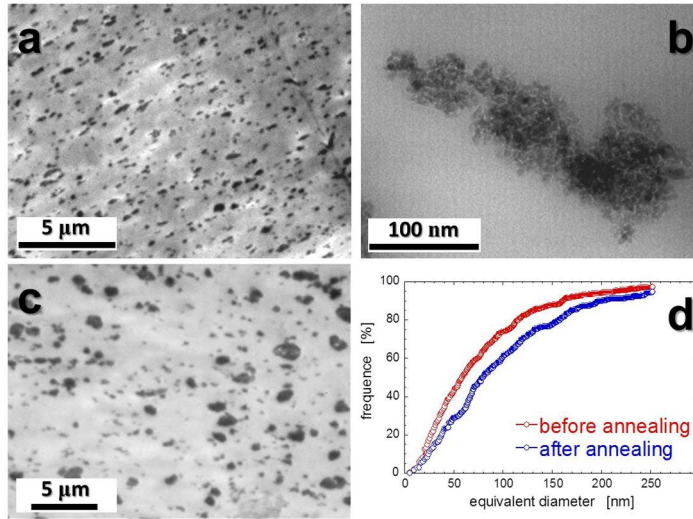


Figure 1. (a) TEM micrograph of the as extruded sample PP/TiO₂ at $\Phi=0.045$. (b) Magnification of an aggregate of TiO₂ nanoparticles. (c) TEM micrograph of the same sample as in (a) after a three-hours thermal annealing at T=190°C. (d) CSD of the samples shown in (a) and (c)(images taken from Acierno et al., 2007a).

The sample was subjected to a thermal annealing at 190°C in quasi-quiet conditions, i.e. by submitting it to shear oscillations in the rheometer at small strain amplitude ($\gamma=2\%$) and frequency ($\omega=0.063 \text{ rad s}^{-1}$). This allows to monitor the evolutions during time of slow dynamic populations, relaxing in timescales of order of $\tau=1/\omega\approx 16 \text{ sec}$, without altering the internal structure of the sample.

The microstructure of the annealed sample is shown in Figure 1.c. A visual comparison with the morphology of the as extruded sample reveals the presence of bigger aggregates and the disappearance of the smaller ones. An analysis of the TEM micrographs was carried out to

quantify the effect of the thermal annealing. An equivalent diameter for the aggregates was defined as $D_i = (\pi A_i)^{0.5}$, where A_i is the measured area of the i -th cluster. Once the sizes of the aggregates are available, the cumulative size distribution (CSD) and the number average size of the TiO₂ aggregates, $D_n = \sum n_i D_i / \sum n_i$ (n_i clusters with size D_i), was determined for each sample. The comparison between the CSDs is shown in Figure 1.d. The lowering of the cumulative CSD curves indicates an increase of the cluster sizes occurred during the thermal conditioning. In particular, the average size of the TiO₂ aggregates increases from $D_n \approx 125$ nm to $D_n \approx 170$ nm.

The coarsening of the microstructure is a consequence of the diffusion of the clusters driven by Van der Waals attraction. Rheological parameters such as the linear viscoelastic moduli are extremely sensitive to the internal microstructure. Thus, we use them to follow such internal rearrangements. The time evolutions of G' and G'' at $\omega = 0.063$ rad s⁻¹ are shown in Figure 2.

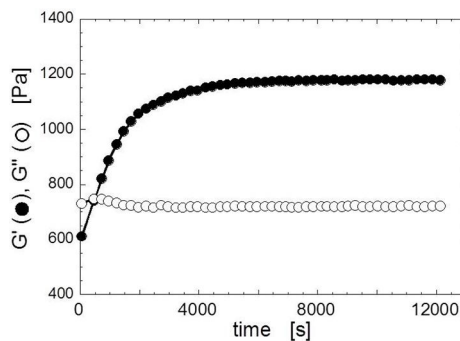


Figure 2. Time evolution of G' (full) and G'' (empty) at $\omega=0.063$ rads^{-1} and $T=190^\circ\text{C}$ for the nanocomposite PP/TiO₂ at $\phi=0.038$ (image taken from Romeo et al., 2009).

The elastic modulus, which is lower than the viscous one at the beginning of the test, increases during the first stage and then it reaches a plateau after a certain time; on the other hand, the loss modulus remains essentially constant. Preliminary investigations revealed that the neat matrices display a constant value of the moduli in the analysed time window. Thus, the increase in the sample elasticity is related to the structuring of the inorganic phase. The characteristic timescale for such a phenomenon can be roughly estimated as the Smoluchowski time for two clusters of radius R to come in contact, τ_a [Russel et al., 1989]. This time depends on the self-diffusion time of each aggregate, given by Equation 2, and on the average inter-aggregates distance, inversely proportional to the filler amount:

$$\tau_a = \frac{\pi\eta_s R^3}{\bar{\phi}k_B T} \quad (4)$$

$\bar{\phi}$ is the actual filler volume fraction, i.e. the volume of the particles in a cluster plus the free volume enclosed between them. These regions are actually inaccessible to the polymer, and depends on how primary particles are assembled together inside the aggregates. As shown in

Figure 1.b, the TiO₂ clusters appear rather compact. As a consequence, we can reasonably assume that the primary particles are packed at a volume fraction of ~60%, which is close to random close packing. The actual filler volume fraction of the PP/TiO₂ nanocomposites can be consequently estimated as $\bar{\phi} \approx \Phi/0.6$. Assuming $R = D_p/2 \approx 65$ nm, Equation 4 gives $\tau_a \sim 4 \times 10^3$ s, in good agreement with the data shown in Figure 2. This result suggests that the increasing of the sample elasticity during time is related to cluster-cluster aggregation. In order to support the previous conclusion, we increase τ_a by increasing either the size of primary particles or aggregates or the viscosity of the suspending medium. According to Equation 2, in these conditions we expect that the elasticity of the samples cannot increase significantly because of the reduced particle mobility.

As first test, we investigate the time evolutions of the linear viscoelastic moduli at $\omega = 0.063$ rad s⁻¹ for a PP/TiO₂ microcomposite (particles radius $R \approx 2$ μm) at $\Phi \approx 0.035$. Based on Equation 4, we expect that two micron-sized particles should come at contact after timescales of order of $\sim 10^7$ s. As a matter of fact, the results shown in Figure 3.a indicate that both moduli remain stable during the aging test until $\sim 10^4$ s.

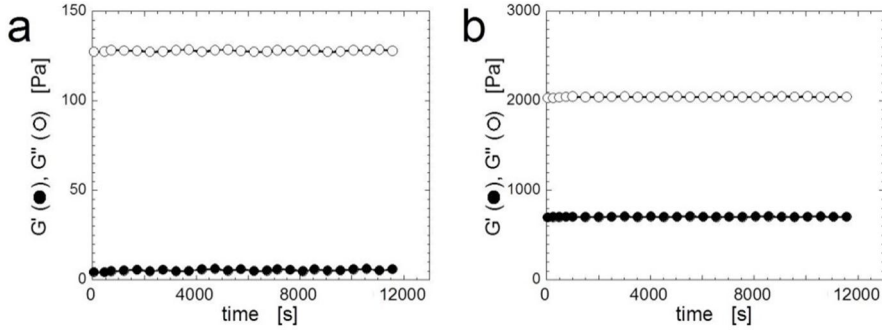


Figure 3. Time evolution of G' (full) and G'' (empty) at $\omega=0.063 \text{ rad s}^{-1}$ for the microcomposite PP/TiO₂ at $\Phi=0.035$ and $T=190^\circ\text{C}$ (a), and the nanocomposite PS-high/SiO₂ at $\Phi=0.035$ and $T=200^\circ\text{C}$ (b)(images taken from Romeo et al., 2009).

As second test, we monitor the moduli of ananocomposite based on a high viscosity matrix such as PS-high ($\eta_0=2.1 \cdot 10^4 \text{ Pa}\cdot\text{s}$ at 200°C) filled with SiO₂ particles at $\Phi \approx 0.035$. Silica aggregates exhibit the typical open and branched structure of fractal objects. In such systems the mass M scales with length L as $M \sim L^{d_f}$, d_f being the fractal dimension [Weitz & Oliveira, 1984]. The actual filler volume fraction thus becomes [Wolthers et al., 1997]:

$$\bar{\Phi} = \Phi \times (L/d)^{3-d_f} \quad (5)$$

Setting $L=D_n \approx 125 \text{ nm}$ as emerged from the analysis of many TEM micrographs, and taking $d_f=2.2$ as a typical fractal dimension of fumed silica aggregates [Kammler et al., 2004], Equation 4 gives $\tau_a \sim 10^5 \text{ s}$. This is

in agreement with the results of the time sweep experiment shown in Figure 3.b, which indicate that cluster assembling phenomena, if any, are negligible in the timescale of the test. Obviously, the not structured sample keeps a predominantly viscous connotation, i.e. $G'' \gg G'$.

Particle rearrangements eventually give rise to mesoscopic structures, such as branched aggregates or space-spanning filler network, which strongly alter the frequency response of the sample. The ω -dependent G' and G'' of two PP/TiO₂ samples filled with micro- and nanoparticles both at $\Phi \approx 0.035$ are compared in Figure 4.a. In both cases the matrix governs the high-frequency response. This suggests that the relaxation modes of the polymer chains and sub-chains are only slightly affected by the presence of the filler at these high frequencies. The presence of microparticles negligibly affects the whole response of the composite. On the contrary, the nanoparticles significantly alter the low-frequency moduli of the material, and in particular the elastic one.

The flattening of G' over long timescales is a general feature characterizing different kinds of PNCs [Krishnamoorti & Yurekli, 2001; Du et al., 2004]. Such a behaviour, however, is not a direct consequence of the nanometric size of the particles, but rather it originates from particle mobility. To emphasize this point, in Figure 4.b the frequency response of the three-hours aged samples PS-low/SiO₂ and PS-high/SiO₂ at $\Phi \approx 0.035$ are compared. The nanocomposite with high viscosity matrix displays a liquid-like behaviour at low frequency reminiscent of

that of the neat polymer (not shown). Differently, the PS-low/SiO₂ sample exhibits a predominant elastic connotation, the low-frequency plateau of G' being indicative of the presence of a space-spanning filler network formed during the ageing process.

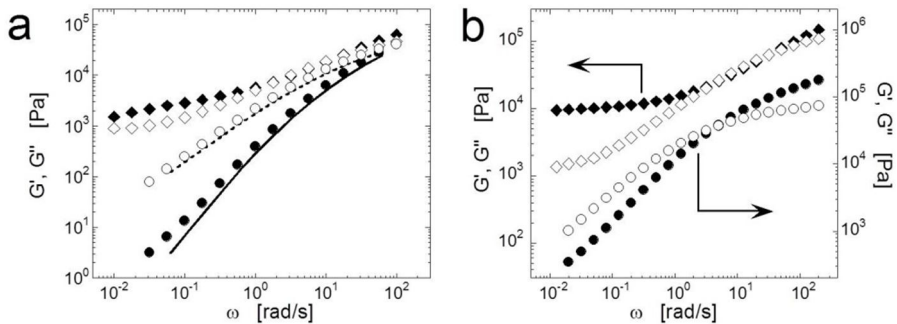


Figure 4. (a) G' (full) and G'' (empty) for the samples PP/TiO₂ at $\Phi \approx 0.035$ filled with micrometric (circles) and nanometric (diamonds) particles. Solid and dashed lines represent the elastic and viscous modulus of the neat PP, respectively. (b) G' (full) and G'' (empty) for the nanocomposite samples PS-low/SiO₂ (diamonds, left axis) and PS-high/SiO₂ (circles, right axis) at $\Phi \approx 0.035$ (image reprinted from Romeo et al., 2009).

To summarize, the viscoelastic response of a filled polymer is greatly affected by particle mobility. When the characteristic diffusion time of the particles and/or aggregates resulting from the extrusion process is too high, either because the matrix is too viscous or the particle size is too big, the filler is unable to rearrange and only produce a small perturbation of the composite viscoelastic response. Conversely, when mobility of the inorganic phase is high enough, random motion and

attractive Van der Waals forces lead to the structuring of the primary aggregates. This eventually results in the formation of a whole space-spanning filler network. Since this network exhibits the connotation of an elastic solid, a drastic slowing down of relaxation dynamics occurs at low frequencies.

2.4 Linear viscoelasticity of PNCs

2.4.1 Weakly attractive particles suspended in Newtonian fluids – A two-phase model

Colloidal suspensions are typically nanometer to micron sized particles dispersed in a medium. They usually exhibit a wide spectrum of rheological properties, ranging from simply viscous fluids to highly elastic pastes depending on the amount of particles and the sign and magnitude of inter-particles interactions. Here we are interested in weakly attractive systems, where the particles are favourable to assemble together into branched aggregates. In these systems, the ω -dependent storage and loss modulus typically exhibit a strong dependence on both Φ and U . Such a high variability makes extremely difficult a general description of the viscoelastic behaviour of colloidal dispersions. A drastic simplification has been introduced by Trappe and Weitz, which showed that a model of a solid network interspersed in a

purely viscous fluid (two-phase model) qualitatively accounts for the viscoelasticity of their samples [Trappe & Weitz, 2000]. The authors studied dispersions of carbon black in base stock oil as a function of particle volume fraction and interaction potential. The U was tuned by adding a dispersant that acts as a surfactant. Without dispersant carbon black particles are rather strongly attractive, and flocs of $\sim 100 \mu\text{m}$ in size form even at very low amounts of particles. The linear viscoelastic moduli of samples at different Φ were measured as a function of frequency with a strain-controlled rheometer with Couette geometry. The authors found that a rheological transition occurs at $\Phi_c = 0.053$: at $\Phi > \Phi_c$ the suspension is clearly elastic and G' is nearly independent on ω ; at $\Phi < \Phi_c$ the viscous feature definitely prevails over the elastic one, and the suspension rheology is very close to that of the suspending fluid. Microscopic analyses reveal that the rheological transition reflects the state of dispersion of the filler: isolated carbon black flocs are suspended in the background fluid below Φ_c , whereas above this threshold the aggregates assemble in a three-dimensional space spanning network.

Despite their marked differences, the moduli of the samples at $\Phi > \Phi_c$ can be scaled onto a single pair of master curves. The authors qualitatively accounted for the observed scaling by assuming that the carbon black forms a solid but tenuous network with a purely elastic, ω -independent modulus. The elasticity of this network, G'_0 , increases with Φ as the

network becomes more and more robust. Interspersed throughout this structure is the purely viscous suspending fluid, which G'' linearly increases with ω and is substantially independent of Φ . Consequently, the elasticity of the network prevails at low ω , while the viscosity of the fluid dominates at high ω . Within this simplified picture, scaling the elasticity of each sample along the viscosity of the matrix results in the collapse of data of samples at different composition onto a single pair of master curves.

Although the proposed approach can account for the basic scaling behaviour, many issues remain unresolved. For example, the behaviour of the weaker of the two moduli in each regime is not addressed. At low frequencies, $G''(\omega)$ must be determined by the loss modulus of the network, which is larger than that of the suspending fluid. Similarly, at the highest frequencies $G'(\omega)$ must reflect the storage component of the suspending fluid with the solid network in it. In addition, the model does not take into account hydrodynamic effects. Despite these limitations, the good quality of the scaling supports the reliability of the approach, indicating that there is a strong similarity in the structures of the networks that form at different Φ . This also implies some predictive feature of the model: the tiny elasticity of samples at low Φ (as long as greater than Φ_c), which networks are too tenuous to be appreciated through direct dynamic-mechanical analyses, can be predicted with good approximation by simply referring to the master curve of G' .

2.4.2 Weakly attractive nanoparticles suspended in non-Newtonian mediums – Recovering the two-phase model

The relatively high mobility of nanoparticles even in highly viscous fluids such as polymer melts makes PNCs similar to colloidal dispersions. The main difference with these simpler systems is the non-Newtonian feature of the suspending medium. According to Trappe and Weitz, the viscoelasticity of a colloidal suspension above Φ_c originates from the combined responses of an *elastic* particle gel that of the *purely viscous* background fluid. In the case of a PNC, instead, the suspending medium is viscoelastic by itself, and its response combines with that of the space-spanning network giving rise to a much complex ω - and Φ -dependent viscoelastic behaviour. It follows that a separation of the effects of the solid and fluid phases is no more possible in the case of PNCs. However, we argue that a recovery of the two-phase model is possible if the elasticity of the polymer is neglected with respect to that of the filler network. Under this assumption, the viscoelasticity of the PNC can be split into the independent responses of an *elastic* particle network and that of the *predominantly viscous* polymer. The former contribution depends on the filler content and governs the long timescale response of the composite, whereas the latter is responsible for the high-frequency behaviour (Figure 5).

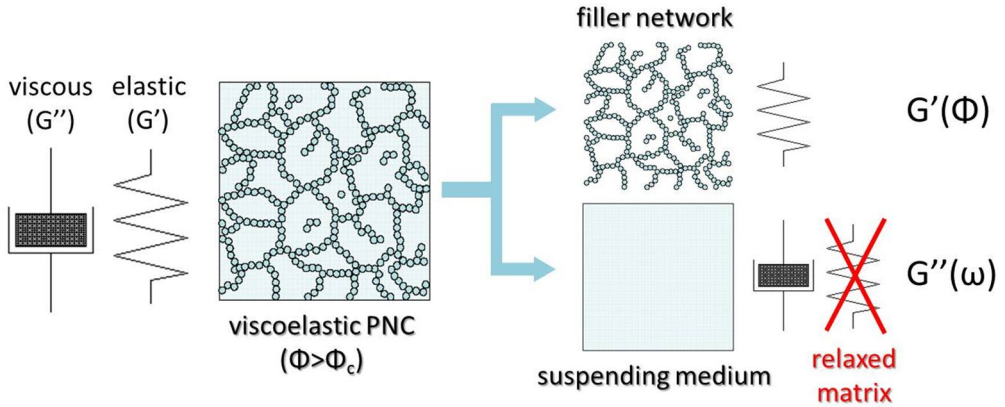


Figure 5. Scheme of the viscoelasticity of a PNC at $\Phi > \Phi_c$. For fully relaxed polymer matrix, the filler network is the only responsible for the elastic connotation of the system.

To test the validity of the previous considerations, we focus on the ω -dependence of the moduli of PP/TiO₂ and PS-low/SiO₂ nanocomposite samples at $\Phi > \Phi_c$, i.e. in which the filler rearranges in experimentally accessible timescales forming a space-spanning network. All these samples share a similar pseudo solid-like behaviour at low frequency, with weak ω -dependences of both moduli and G' greater than G'' . Since the filler mainly affects the elastic modulus of the samples, G' increases with Φ more rapidly than G'' . As a consequence, G' and G'' further cross at intermediate frequencies in addition to the high ω crossover related to the relaxation of the neat polymer matrices. The coordinates of such additional crossing point, $(\omega_c; G_c)$, shift towards higher and higher

frequencies and moduli with increasing the filler content. This is shown in Figure 6 for three samples PS-low/SiO₂ at different composition.

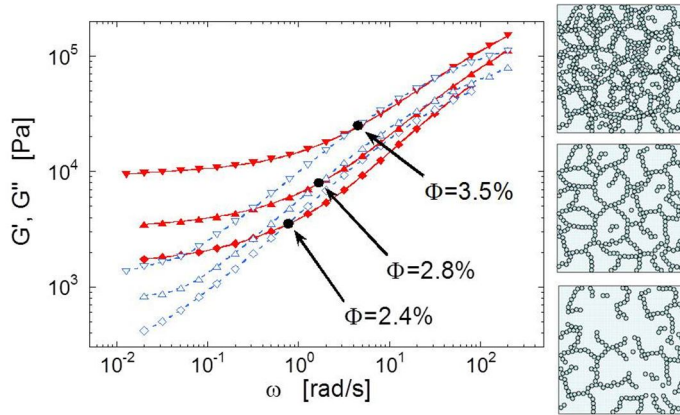


Figure 6. G' (full, red) and G'' (empty, blu) for the nanocomposite samples PS-low/SiO₂ at increasing filler content. The additional crossover is indicated by the arrows.

The low-frequency crossover can be interpreted as the point at which the network elasticity equals the viscous contribution of the polymer. As a consequence, normalizing the moduli of samples at different Φ by their elasticity, and doing so along the background fluid viscosity, the curves should collapse onto a single pair of master curves. Accordingly, the scaling has to be done by shifting the curves both horizontally and vertically using as shift factors $a=1/\omega_c$ and $b=1/G_c$, respectively. The resulting master curves are shown in Figure 7 for both the PP/TiO₂ and PS-low/SiO₂ nanocomposites.

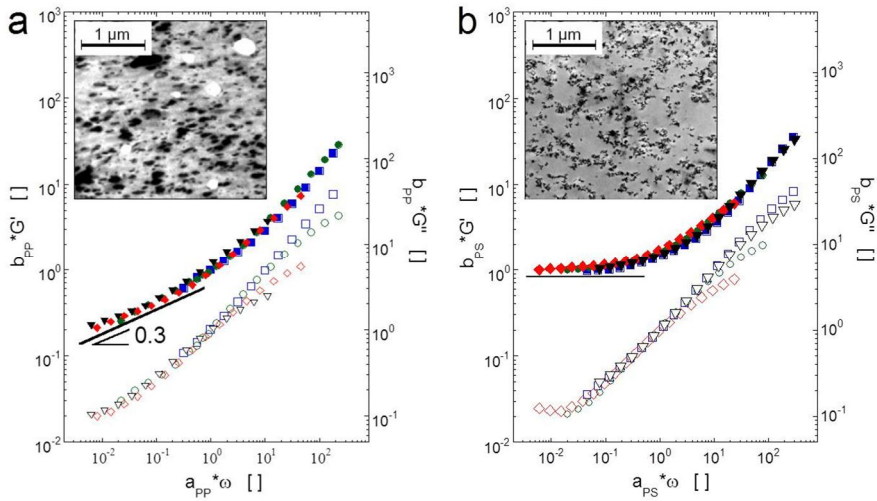


Figure 7. Master curves of G' (full, left axis) and G'' (empty, right axis) for the systems PP/TiO₂ (a) and PS-LOW/SiO₂ (b). Each colour corresponds to a composition. Note that only curves at $\Phi > \Phi_c$ have been used to build the master curves. The TEM micrographs shown in the insets represent the microstructures of samples at $\Phi \approx 0.035$ (image reprinted from Romeo et al., 2009).

The scaled moduli lie on top of each other in about five decades of frequencies, supporting the validity of the adopted approach. Deviations are observed for the viscous moduli at high scaled frequencies. This is not unexpected, since the relaxation modes of the polymers are independent on the filler content and cannot be scaled using a and b as scaling factors.

Once the master curves are built, the differences in elasticity and dynamic of the particle networks become evident. The SiO₂ network is characterized by an ω -independent elastic modulus at low frequency,

which emphasizes its truly solid-like feature. Differently, the TiO₂ network displays a slow relaxation dynamic with $G' \sim \omega^{0.3}$. These differences are related to the differences in network structures formed in the two composites. The TEM images reported in the insets of Figure 7 show that the SiO₂ nanoparticles form a tenuous, fractal network of sub-micron sized, branched floccs interspersed within the host PS. Differently, the TiO₂ nanoparticles are assembled into dense clusters, whose mobility is presumably slowed down by the surrounding aggregates. The transient character of the latter network emerges as a glassy-like decrease of G' , which reflects the internal rearrangements of the TiO₂ clusters. Such slow relaxation dynamics are characteristic of colloidal glasses [Shikata & Pearson, 1994; Mason & Weitz, 1995] and has been observed in many other soft materials [Sollich et al., 1997].

2.4.3 Refining the two-phase model – Role of the hydrodynamic effects

Despite the good quality of the scaling shown in Figure 7, unresolved issues exist regarding the physical meaning of the shift factors. The underlying physics of the model lies on the independent rheological responses of the neat polymer and the particle network. Actually, the coordinates of the crossover point of the moduli of the nanocomposite, identified by Trappe and Weitz as the shift factors for their system, do

not rigorously reflect the properties of the two pristine phases of the model. In addition, the presence of the particles implies hydrodynamic effects, which cannot be eluded for a correct scaling of the data. To account for these issues, the procedure to get the shift factors for the building of the master curve has to be revisited. For this aim, hereinafter we only refer to the system PS-low/SiO₂, which particle network exhibits a truly solid-like behaviour at low frequency.

Hydrodynamic effects reflect the perturbation of the flow lines in proximity of the filler. In a liquid filled with a solid particulate, the suspending fluid flows in the narrow gap between contiguous particles or aggregates, locally experiencing a greater flow rate than what externally imposed or measured. Gleissle and Hochstein quantitatively accounted for hydrodynamic effects in oscillatory shear experiments by introducing an empiric amplification factor, representing the ratio between the complex moduli of the filled sample over that of the neat matrix: $B(\Phi) = G^*(\Phi)/G_{ps}^*$ [Gleissle & Hochstein, 2003]. In the case of microparticles, $B(\Phi)$ well describe the increase of G^* of the suspension in the whole range of accessible frequencies. Differently, non-continuum effects emerge over long timescales in the case of PNCs. Consequently, the hydrodynamic effects only are appreciable at high frequencies, i.e. where the rheological response is governed by the polymer matrix. This is shown in Figure 8, where the complex moduli of

various PS-low/SiO₂ nanocomposites at different composition are reported together with the resulting $B(\Phi)$.

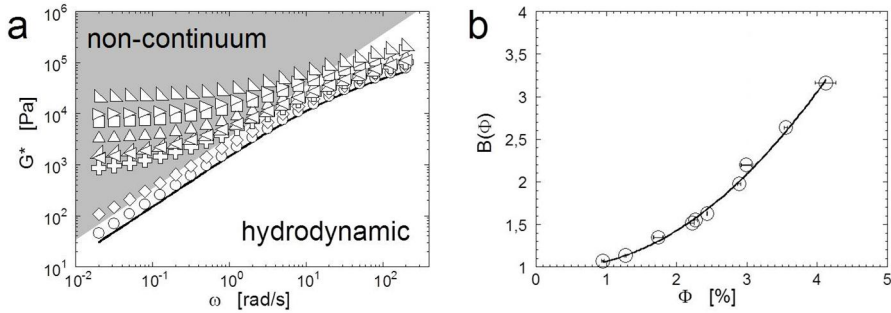


Figure 8.(a) Complex modulus of PS-low/SiO₂ nanocomposite at various filler content. The regions in which non-continuum and hydrodynamic effects are dominant are emphasized. (b) Amplification factor for the data shown in (a) (images taken from Filippone et al., 2010).

After the hydrodynamic contribution has been quantified for each sample, new, more rigorous shift factors can be identified. Specifically, we now refer to the point at which the elasticity of the filler network, given by the plateau modulus of the nanocomposite, $G'_o(\Phi)$, equals the viscous modulus of the neat matrix amplified by $B(\Phi)$ to account for hydrodynamic effects, $B(\Phi) \cdot G^*$.

The comparison between the old (a ; b) and new (a' ; b') shift factors is shown in Figure 9.a for the sample at $\Phi=2.9\%$; in Figure 9.b the new master curve is reported.

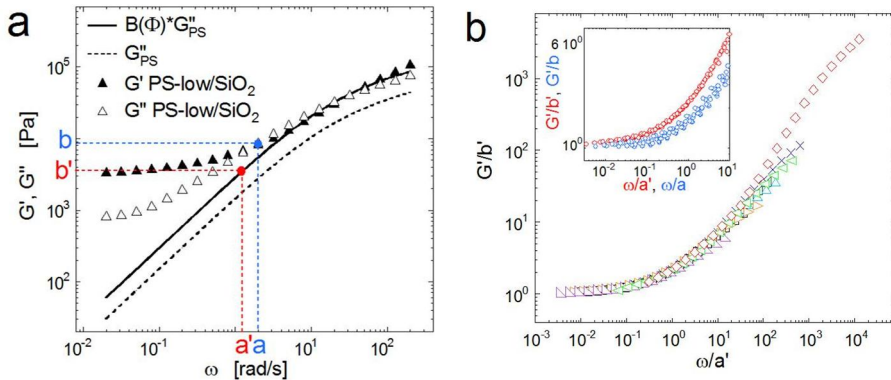


Figure 9. (a) Comparison of the shift factors for the samples-low/SiO₂ at $\Phi=2.8\%$. (b) Master curve of G' built using a' and b' as shift factors; the inset shows a magnifications at low scaled frequencies of the master curves obtained using as shift factors (a' ; b') (red) and (a ; b) (blu) (images taken from Filippone et al., 2010).

The elastic moduli scaled using a' and b' as shift factors lies on top of each other over about seven decades of scaled frequencies, confirming the validity of the adopted approach. Again, the slight deviations at ω/a' greater than $\sim 10^1$ do not invalidate the consistency of the scaling, being a consequence of the intrinsic viscoelastic feature of the suspending fluid.

Besides exactly capturing the underlying physics of the two-phase model, the refined model guarantees a better scaling of the elasticity of samples at different composition. This is shown in the inset of Figure 9.b, where the master curves built using the two sets of shift factors are compared. The lower scattering of the data scaled using a' and

b' confirms the importance of properly accounting for hydrodynamic contributions when dealing with PNCs.

2.5 Strength and reversibility of the filler network in PP/Al₂O₃ PNCs

Aim of this paragraph is the study of the relationships between the rheology and structure of PP/Al₂O₃ nanocomposites. The structuring (during a quiescent annealing process) and de-structuring (promoted by large amplitude shear flows) of the filler network are investigated by means of both rheological and TEM analyses. The internal morphology of the sample PP/Al₂O₃ at $\Phi=4.2\%$ at the end of the extrusion process is shown in Figure 10.

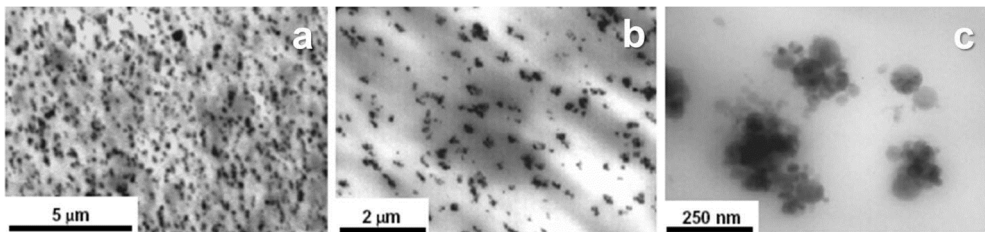


Figure 10. TEM micrographs of the as extruded PP/Al₂O₃ sample at $\Phi=4.2\%$ at various magnifications (image taken from Acierno et al., 2007b).

Although a homogeneous distribution can be observed on microscale, the presence of aggregates of a few hundred nanometers is noticed at higher magnifications. The aggregates appear as open structures

formed of tens of nanospheres of different sizes. Such non-equilibrium structures rearrange towards a more favourable thermodynamic state during a subsequent aging above the PP melting temperature. The morphology of a sample at $\Phi=4.2\%$ after a 3-hours annealing at $T=190^\circ\text{C}$ is shown in Figure 11.

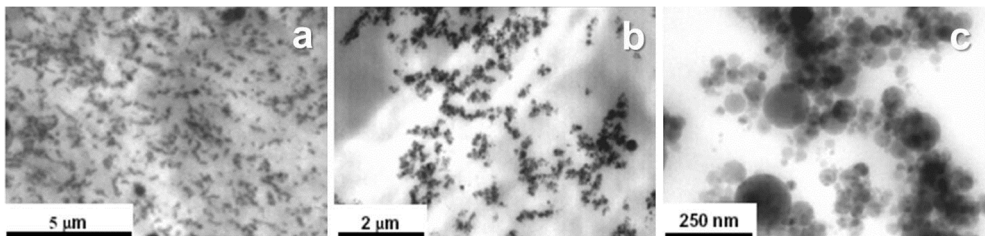


Figure 11. TEM micrographs of the 3-hours thermal annealed PP/Al₂O₃ sample at $\Phi=4.2\%$ at various magnifications (image taken from Acierno et al., 2007b).

Pristine individual aggregates are now assembled into a disordered network that spans large sections of the sample. The particles and aggregates are essentially kept together by Van der Waals attractions and/or other kinds of weak bonds between the functional sites located at the particle surfaces. The application of large strains provides an excess energy to overcome such attractive interactions, thus destroying the network. After that, the particles may or may not aggregate again depending on the strength of inter-particle interactions.

The relaxation dynamics of a viscoelastic fluid can be indifferently monitored by frequency scans or stress relaxation tests. In the latter

kind of experiment, a constant strain, γ_0 , is imposed to the sample in the linear regime, and the transient stress, $\sigma(t)$, is measured as a function of time. The stress relaxation modulus, $G(t) = \sigma(t)/\gamma_0$, is shown in Figure 12 after the application of large amplitude oscillatory shear (LAOS) at a constant frequency $\omega = 0.0628 \text{ rad s}^{-1}$ and different γ_0 on the 3-hours aged sample at $\Phi = 4.2\%$.

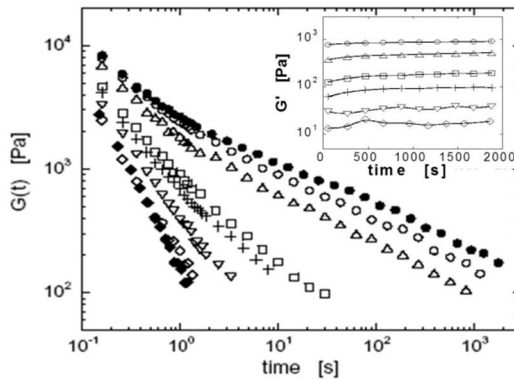


Figure 12. $G(t)$ of the 3-hours aged PP/Al₂O₃ sample at $\Phi = 4.5\%$ after LAOS at different strain amplitudes γ_0 : 0.8% (solid circles), 10% (open circles), 25% (triangles), 50% (squares), 100% (crosses), 250% (reverse triangles), 500% (diamonds). Solid diamonds represents the $G(t)$ of the neat polymer. The time evolutions of G' after each LAOS are shown in the inset. Symbols are the same of stress relaxation moduli (image taken from Acierno et al., 2007b).

Large deformations have a drastic effect on the relaxation spectrum: the more the strain amplitude, the faster the relaxation dynamics. Time sweep tests in linear regime were performed after each LAOS to test the

viscoelastic behaviour of the sheared sample, and the results are shown in the inset of Figure 12. The elastic feature progressively vanishes with increasing the deformation amplitude. Interestingly, the steadiness of the elastic modulus during time suggests an irreversibility of the network break-up process, at least within the experimental time window. Moreover, a polymer-like behaviour is recovered after the LAOS at the largest amplitude ($\gamma_0=500\%$). In such case, the inorganic phase does not affect the rheological response of the nanocomposite at all.

The morphology of the 3-hours aged sample after the LAOS at $\gamma_0=500\%$ is reported in Figure 13. The network formed during aging is no more visible, and the presence of many small clusters characterizes the sheared system. The flocs show a more open structure than that of a not sheared sample, either aged or not, suggesting a weaker tendency to the clustering for the Al_2O_3 nanoparticles after the large deformations. The cumulative cluster size distributions were determined through the analysis of TEM micrographs. The results are shown in Figure 14 for the as extruded, 3-hours annealed and sheared after aging samples at $\Phi=4.2\%$. The number average equivalent diameters of the clusters are reported in the same figure.

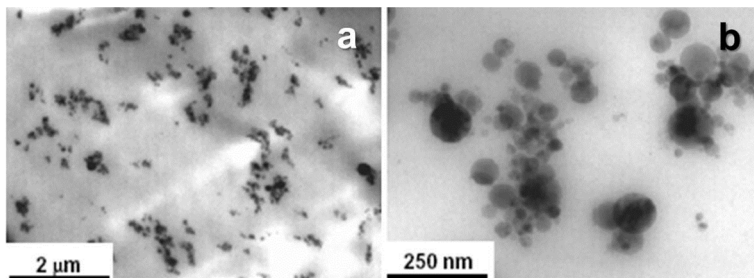


Figure 13. TEM morphology of the 3-hours aged sample at $\Phi=4.2\%$ after the LAOS at $\gamma=500\%$ (image taken from Acierno et al., 2007b).

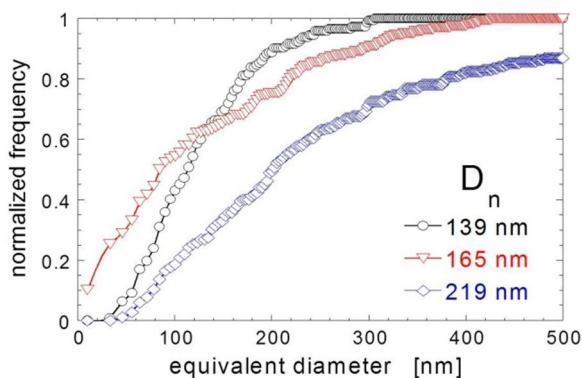


Figure 14. CSDs for the PP/Al₂O₃ sample at $\Phi=4.2\%$ as extruded (black circles), 3-hours aged (blue diamonds) and 3-hours aged after LAOS at $\gamma_0=500\%$ (red triangles) (image taken from Acierno et al., 2007b).

The CSD of the as extruded sample is rather sharp, indicating a good dispersion efficiency of the extrusion process. The thermal annealing results in a significant widening of the CSD, with the appearance of very large clusters (D_n greater than 800 nm). This confirms the metastable feature of the samples, which quickly evolve toward states of less free

energy under the push of the inter-particle attractive interactions. The resulting filler network breaks up when the sample is subjected to LAOS, and a remarkable sharpening of the CSD is observed.

Interestingly, the strength of the filler network depends on whether the LAOS is applied before or after the thermal annealing. This is shown in Figure 15, where the loss factor $\tan\delta = G''/G'$ (15.a) and the complex moduli (15.b) of the samples at $\Phi=4.2\%$ submitted to LAOS ($\gamma_0=500\%$) are reported before and after the ageing; the curves of the 3-hours aged but not sheared sample are also reported for comparison.

If the LAOS is applied to the sample before the formation of the particle network, the system quickly evolves to a more elastic structure, the $\tan\delta$ asymptotically reaching values close to those of the not sheared sample. However, the comparison between the G^* shown in Figure 15b reveals that the strength of the network formed after the LAOS is much lower than that of the not sheared sample.

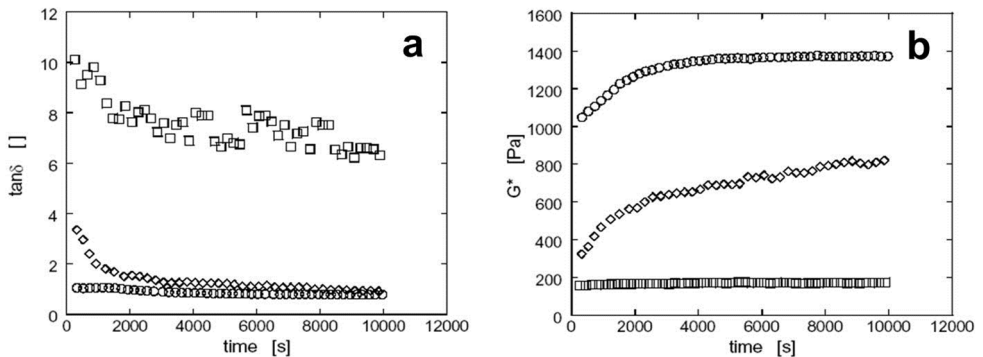


Figure 15. Loss factor (a) and complex moduli (b) of the samples at $\Phi=4.2\%$ submitted to LAOS ($\gamma_0=500\%$) before (diamonds) and after (squares) the thermal annealing. The curves of the 3-hours aged and not sheared sample (circles) are also reported for comparison (image taken from Acierno et al., 2007b).

Such a result can be explained by assuming some rearrangement of the reactive sites of the particle surfaces after the network break-up, which may weaken the surface activity of the particles. This reduces the intensity of inter-particle interactions and, as a consequence, the strength of the filler network [Bicerano et al., 1999]. On the other hand, if a "strong" network forms and then is destroyed by LAOS, the restoration of new bonds required for the reformation of the network can result inhibited. This could explain the irreversibility of the structuring process noticed after the LAOS performed on the aged sample.

2.6 Conclusions

The effect of small amounts of nanoparticles on the melt-state linear viscoelastic behaviour has been investigated for different polymer-nanoparticles model systems characterized by poor polymer-particles interactions and low particle contents. The drastic increase of the rheological properties with respect to the matrices has been related to

the formation of a filler network above a critical particles volume fraction. This is a consequence of particles and clusters rearrangements taking place during a thermal annealing. The filler mobility depends on both particle size and viscosity of the suspending medium. Once formed, the filler network exhibits an elastic feature that mixes with the intrinsic viscoelastic response of the polymer matrix, resulting in a complex Φ - and ω -dependent viscoelastic response of the nanocomposite. However, starting from a two-phase model proposed for colloidal suspensions in Newtonian fluids, we have shown that the contributions of filler network and suspending medium can be decoupled due to the weak polymer-particle interactions and the differences in temporal relaxation scales. The adopted approach has been validated through the building of a mastercurve of the moduli, which reflects the scaling of the elasticity of composites along the viscosity of the suspending medium. The two-phase model well worksirrespective of the structure of the filler network, making evident the strict interrelationships between the structure, both on nano- and micro-scale, and themelt-state behaviour of the studiedPNCs.The physical meaning of the two-phase model clearly emerges once hydrodynamic effects have been properly taken into account. Besides clarifying the various timescales ofPNCs, the proposed model allows for predicting the modulus of particle networks which are too tenuous to be appreciated through simple frequency scans. The application of a

large amplitude oscillatory shear flows provides an excess energy for the system to escape from the metastable configuration in which it is trapped. This destroys the network formed during the thermal annealing, leading to a more tenuous structure which is unable to significantly contribute to the system elasticity. After the network has been destroyed the sample cannot recover its previous solid-like feature during a subsequent thermal annealing. This is probably due to some rearrangement of the reactive sites of the particle surfaces occurring after the rupture of the inter-particles bonds formed during annealing. Besides well describing the behaviour of PNCs in the framework of simpler systems such as Newtonian colloidal suspensions, the analysis proposed in this chapter is expected to be useful to understand a wide variety of complex fluids in which a superposition of the elasticity of the components is possible. The generalization of our approach to such systems and to other technologically relevant PNCs, such as nanocomposites based on layered silicates or carbon nanotubes, still remains to be proved.

Chapter 3

Scaling the Melt-Elasticity of Interacting Polymer Nanocomposites

*Universal Features of PEO/SiO₂ Mixtures at Different
Filler Content and State of Dispersion*

3.1 Introduction

Adding solid particles is a common way to improve the macroscopic properties of commodity plastics. The structure of the resulting composite can be described as a suspension of particles or particle aggregates dispersed in the polymer matrix. Interactions between individual particles/aggregates and the matrix, as well as between particles, hinder the relative motion between material planes modifying both the solid- and melt-state behaviour of the host polymer. In polymer-based microcomposites, these effects only become relevant at

high filler contents, i.e. when the particles are sufficiently close to each other to form a network that spans large sections of the matrix. Over the last twenty years the same reinforcing effects have been observed upon addition of very low amounts of inorganic nanoparticles, which has resulted in extensive research in the field of polymer-based nanocomposites (PNCs)². The unique features of PNCs originate from the extremely high area-to-volume ratio of the filler, which results in significant interfacial areas between the polymer and the particles. Such large interphase enables a substantial fraction of polymer to directly interact with the particles, resulting in noticeable effects on the macroscale properties of the composite even for very low filler loadings. For particle volume fractions ϕ as low as 10%, nanometric average inter-particles distances are expected for well-dispersed nanocomposites³. This means that, if the particle radius approaches the mean polymer radius of gyration, R_g , each single chain interacts on average with more than one nanoparticle⁴. Taking into account the high mobility of nano-sized particles even in highly viscous mediums such as polymer melts⁵, two scenarios are hence possible: if good affinity exists between the polymer and the filler, then a polymer-mediated transient network establishes between the particles⁶⁻⁹; on the other hand, in case of weak polymer-filler interactions, the nanoparticles aggregate in the melt and form flocs, which eventually assemble into a whole space-spanning network¹⁰⁻¹³. In both cases, the presence of a three-

dimensional stress-bearing superstructure has a profound effect on the composite rheology, and the polymer melt is converted into a self-supporting material with a predominant elastic response. The dependence of such elasticity on filler loading is a complex function of several parameters, such as the initial state of dispersion, the interfacial characteristics, as well as the mechanisms governing aggregation and stress bearing. As a consequence of the intrinsic inhomogeneity on nanoscale, continuum rheological models fail in capturing the complex response of PNCs, and a general description of the physical relationships between structure and macroscopic properties of such systems is still lacking. A two-phase model has been recently proposed to describe the linear viscoelasticity of PNCs with negligible polymer-particle interactions^{14,15}. The underlying physics of the model is based on the independent responses of two main dynamical species: the predominantly viscous polymeric matrix and the purely elastic particle network that forms above the percolation threshold. Using the same approach, in the present paper we investigate systems characterized by non-negligible polymer-particle interactions. Specifically, we deal with PNCs based on a mixture of poly(ethylene-oxide) (PEO) and fumed silica (SiO₂) nanoparticles prepared using two different compounding procedures, resulting in different states of dispersion of the particles. The polymer-filler interactions are dictated by hydrogen bonding between the silanol groups on the particle surface and the ether groups

on PEO backbone¹⁶⁻¹⁸. Scaling the linear elastic moduli of samples at different composition allows to build a single master curve, demonstrating the ability of the two-phase model to successfully capture the linear viscoelastic behaviour even for interacting systems. The analysis of the scaling factors highlights similarities in the melt state dynamics of the systems prepared with the two compounding procedures. Further, irrespective of the state of filler dispersion, the elasticity of all samples exhibits critical behaviour in the proximity of the percolation threshold, with critical exponent values close to those predicted for polymer-bridged gels.

3.2 Experimental

3.2.1 Raw materials

The PEO, purchased from Sigma-Aldrich and used as received, has weight-average molecular weight $M_w=100$ KDa, glass transition temperature $T_g=-67^\circ\text{C}$ and melting temperature $T_m=60^\circ\text{C}$. Fumed silica is an amorphous form of silicon dioxide made of primary spherical particles fused together in the form of fractal aggregates of a few hundreds of nanometers¹⁹. The fumed silica used in this work, kindly supplied by Degussa, is the Aerosil® A150, having primary particle size $d=14$ nm, specific surface area $\sim 150\pm 15$ m²/g and bulk density $\rho=2.2$

g/mL. The hydrophilic feature of this kind of filler derives from the silanol groups on the surface of the particles. Mueller et al. reported typical surface density of silanols of 2÷3 groups/nm² for flame-made silica powders²⁰.

3.2.2 Nanocomposites preparation

Two series of nanocomposites at different filler content were prepared using two different procedures.

The samples classified as "MC" were prepared by melt compounding the polymer and the nanoparticles using a co-rotating twin-screw extruder (Minilab Microcompounder, ThermoHaake) equipped with a capillary die (diameter 1.5 mm). The extrusions were carried out at $T=80^{\circ}\text{C}$ under inert gas (N_2) atmosphere at a screw speed of 160 rpm, corresponding to average shear rate inside the extrusion chamber of order of $\sim 80 \text{ s}^{-1}$. A feedback chamber allowed for the accurate control of the residence time, which was set to $\sim 250 \text{ s}$ for each sample. The polymer and the filler were previously dried under vacuum for ~ 16 hours at 50°C . The neat polymers used as reference materials were extruded in the same conditions. Finally, the extruded pellets were compression moulded into disks (diameter 25 mm, thickness $\sim 1.5 \text{ mm}$) using a laboratory press (LP-20B by Lab. Tech. Eng. Company Ltd.).

The samples classified as “FD” were prepared through the following procedure. The nanoparticles were dispersed in distilled water and the suspension was ultrasonicated for one hour and stirred overnight. Then, the PEO was added and dissolved through vigorous stirring for 24 hours at room temperature. The resulting solution was poured into glass dishes, suddenly quenched in liquid nitrogen and freeze-dried for 48 hours to remove the water. The freeze-drying process led to highly porous samples, which were disk-shaped at 80°C in a vacuum oven under very low pressures (~0.1 bars) to obtain compact disk-shaped samples suitable for rheological analyses. A sample based on the neat polymer was prepared using the same procedure and used as reference material for the FD samples.

3.2.3 Characterization

The MC and FD disks were fractured in liquid nitrogen and observed using a field emission scanning electron microscopy (FEG-SEM by FEI, mod. Quanta 200). Energy dispersive spectroscopy (EDS, Oxford INCA X-act energy dispersive analyser) was used to study the state of dispersion of the filler on micro-scale. EDS measures the X-rays emitted during electron beam irradiation of a selected area of the sample, determining its chemical composition. By rastering the electron beam over the area of interest, an X-ray map can be obtained which shows the spatial distribution and relative proportion of previously defined elements. The

fracture surfaces were mapped with respect to the silicon, which is only present in the filler phase.

Rheological analyses were performed using a stress-controlled rotational rheometer (TA Instruments mod. ARG2) in parallel plate geometry (diameter 25 mm). Measurements were carried out at $T=110^{\circ}\text{C}$ in a dry nitrogen atmosphere. Viscoelastic analyses were performed in the linear regime, which was established for each sample through preliminary strain-sweep tests. Low-frequency ($\omega=0.05$ rad/s) time sweep experiments were carried out to investigate the temporal evolution of the linear viscoelastic properties. The moduli reach steady state values in ~ 1 hour, afterwards the relaxation spectra were collected by means of oscillatory shear frequency scans. Due to a marked sensitivity of the rheological properties to the filler content, thermogravimetric analyses (TGA) were performed on the samples recovered at the end of rheological tests. The weight fractions deduced from TGA were converted into volume fractions (ϕ) using the bulk densities of the components.

3.3 Results and Discussion

3.3.1 MC samples: structure and linear viscoelasticity

The melt compounding procedure is expected to ensure a good distribution of the filler on micro-scale. A representative SEM micrograph of the MC sample at $\phi \approx 4\%$ is shown in Figure 1.a. Although well-embedded in the matrix, as a consequence of the affinity between the two phases, the filler is recognizable in the form of sub-micron sized aggregates homogeneously distributed within the host polymer. To inquire about the state of dispersion over larger length scales, a low-magnification SEM micrograph is shown in as it is (Figure 1.b) and with the X-ray map of the Silicon (Figure 1.c). Here the red spots represent the regions where silicon was detected, and indicate that the particles are concentrated in micron- and submicron-sized areas uniformly distributed over the surface.

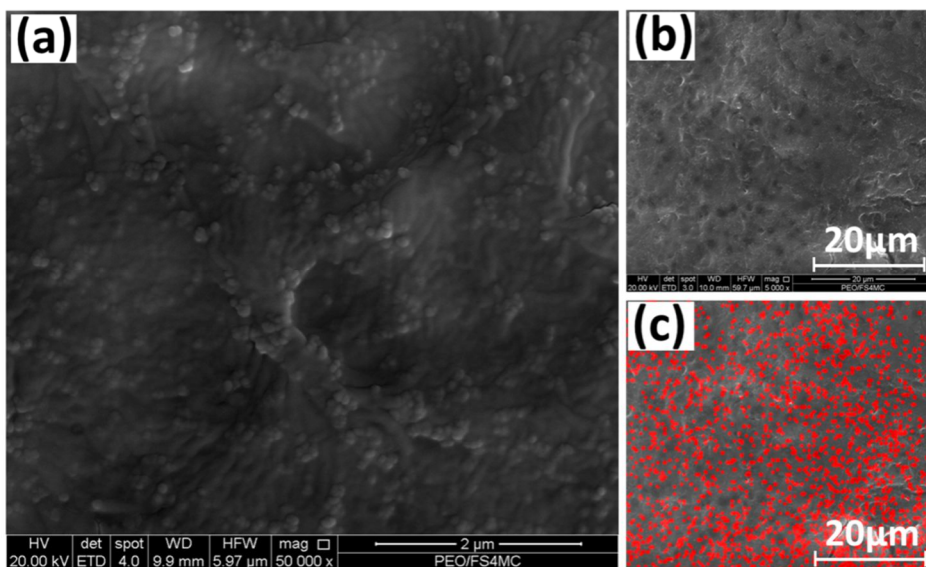


Figure 1. (a) SEM micrograph of the MC sample at $\phi \approx 4\%$. A low magnification SEM is shown in (b); the same micrograph is shown in (c) with the X-ray map of the Silicon superimposed on it.

The visual inspection of the SEM micrographs and the EDS map indicate that the filler in the MC sample is well distributed, though probably not quite as dispersed. The linear viscoelasticity of filled polymers is extremely sensitive to the state of dispersion of the filler and its interactions with the host polymer. The frequency dependence of the linear elastic (G') and viscous (G'') moduli for the MC composites at different filler content is shown in Figure 2.

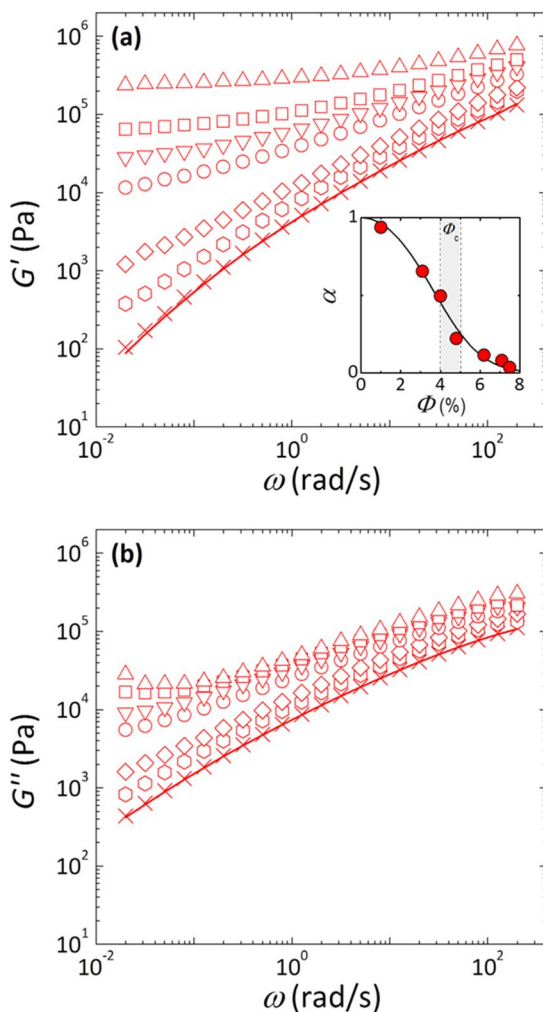


Figure 2. Frequency dependence of the linear elastic (a) and viscous (b) moduli of the neat PEO and the MC samples at different filler content: from bottom to top, $\phi=1\%$, 3.1% , 4% , 4.8% , 6.2% , 7.1% and 7.5% ; the lines are the moduli of the extruded neat PEO. The inset in (a) shows the low frequency log-log slope of $G'(\phi)$ normalized to that of the pure polymer, $\alpha(\phi)$.

The filler strongly affects the relaxation spectrum of the samples. Both moduli monotonically increase with silica content in the whole range of investigated frequencies. The effect is more pronounced on G' . The relaxation dynamics of the composites at high frequencies, however, remind that of the neat matrix, the particles only causing a vertical shift of both moduli by an amount proportional to ϕ_c . Over these short timescales the effect of the filler essentially reduces to a local increase of the shear rate experienced by the matrix in the gaps between particles or aggregates. Gleissle and Hochstein quantitatively account for such hydrodynamic interactions by introducing an amplifying factor $B(\phi)$, representing the ratio between the complex modulus, $G^*=(G^2+G'^2)^{1/2}$, of the filled sample over that of the neat matrix²¹. In the case of non-interacting microparticles, $B(\phi)$ fully describes the apparent increase of the rheological properties of the suspension in the whole range of experimentally accessible frequencies. In the case of aggregating nanoparticles, however, hydrodynamic interactions only emerge at high frequencies, where the behaviour of the polymer matrix governs the rheological response¹⁴. Over longer timescales the presence of the filler determines a gradual slowing-down of the relaxation dynamics, eventually resulting in the arrest of the relaxation processes above a critical filler volume fraction, ϕ_c . The appearance of a low-frequency plateau of G' is not unexpected in nanofilled polymers, and is primarily attributed to the formation of some three-dimensional

percolating network that spans the whole sample. Since $\Phi=5\%$ is the lowest volume fraction at which G' exhibits a predominantly elastic behavior and a low-frequency plateau, we infer that ϕ_c falls in the composition range $4\% \leq \phi_c \leq 5\%$. Such a conclusion is supported by the analysis of the low frequency log-log slope of $G'(\phi)$ normalized to that of the pure polymer, $\alpha(\phi)$, shown in the inset of Figure 2.a. α monotonically decreases with ϕ , reaching a value of about 0.5 at $\Phi \approx 4\%$. At that concentration both G' and G'' scale as $\sim \omega^{0.5}$ over three frequency decades. Such a phenomenology is reminiscent of systems around the gel point²². We therefore conclude that for our MC samples $\phi_c \approx 4\%$.

3.3.2 Linear viscoelasticity: Two-phase model

The linear viscoelasticity of PNCs characterized by negligible polymer-filler interactions above ϕ_c can be modeled as the superposition of the independent contributions of a purely elastic particle network and that of the predominantly viscous polymer matrix^{14,15}. In principle, such model should fail when applied to interacting systems like those studied here, where a substantial fraction of the polymer is expected to be involved in the filler dynamics. Specifically, the adsorption of PEO on the surface of silica particles reduces the mobility of the bound chains due to confinement effects, trapping of the entanglements and polymer bridging^{8,23,24}. As a result, the dynamics of PEO/SiO₂ systems can be highly heterogeneous. However, irrespective of the presence of

adsorbed polymer chains, we argue that the dynamics of the polymer-mediated network are substantially different from those of the free bulk polymer. This allows to separate the contributions coming from these two main dynamical populations and, as a consequence, to recover the two-phase model. To test this idea, we build a master curve of the elastic moduli of the samples at $\phi > \phi_c$ by using the same procedure described by Filippone et al.¹⁴. First, we estimate the amplification factors $B(\phi)$ related to hydrodynamic interactions (Figure 3.a). Then, we identify the horizontal (a) and vertical (b) shift factors as the points at which the network elasticity, set as the low frequency plateau of the storage modulus, $G'_o(\phi)$, equals the viscous modulus of the neat polymer amplified to account for hydrodynamic effects, $B(\phi) * G''_{PEO}(\omega)$. The resulting master curve of G' for the MC composites is shown in Figure 3.c.

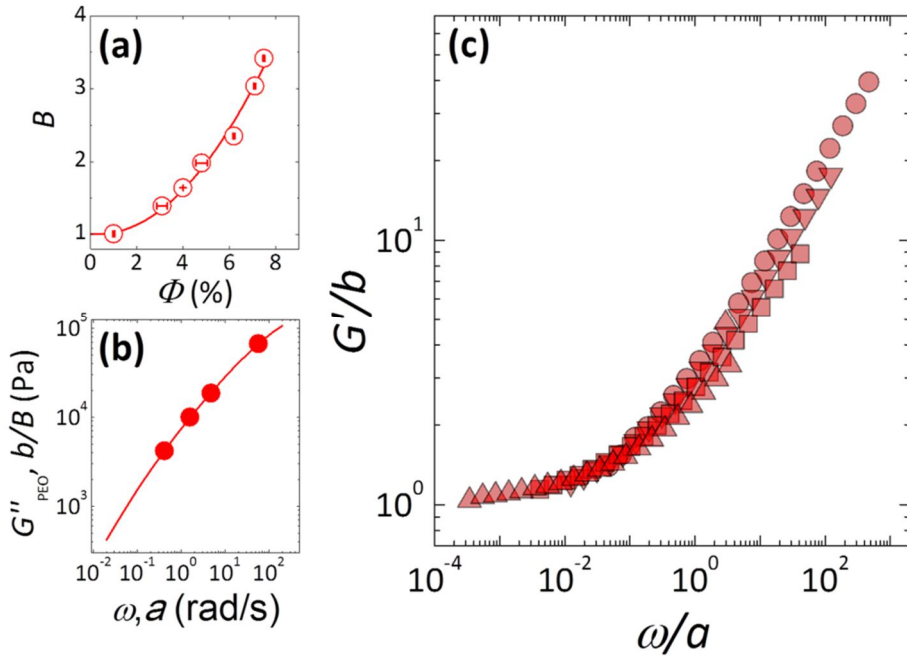


Figure 3. (a) Amplification factors $B(\phi)$ related to the hydrodynamic effects; the line is a guide for the eye. (b) Shift factors used to shift the G' curves, lying on the viscous modulus of the neat PEO. (c) Master curve of G' of the MC samples at $\phi > \phi_c \approx 4\%$; the symbols are the same of Figure 2.

The collapse of the moduli is satisfactory over about four decades of low scaled frequencies. The non-scaling tails at high ω/a do not compromise the quality of the scaling, being related to the relaxation modes of the unfilled matrix, which are totally independent on the filler dynamics.

The good superposition shown in Figure 3.c reflects the consistency of the two phase model. Hence the viscoelasticity of the PEO-SiO₂ composites stems from the combination of the independent response

of a fraction of “free” polymer, and of a much slower superstructure, consisting of particles and adsorbed polymer. The relative amounts of free and adsorbed polymer are expected to depend on the extent of specific particle surface. Specifically, a better dispersion of the filler should result in an increase of the bound fraction, along with a lowering of Φ_c .

3.3.3 *Freeze-Dried* samples: Role of the state of filler dispersion on the linear viscoelasticity

The freeze-drying technique should preserve the high degree of filler dispersion attained during the solution mixing. In Figure 4 a SEM micrograph of the FD sample at $\Phi \approx 4\%$ is shown as it is (a) and with the X-ray map of the Silicon (b).

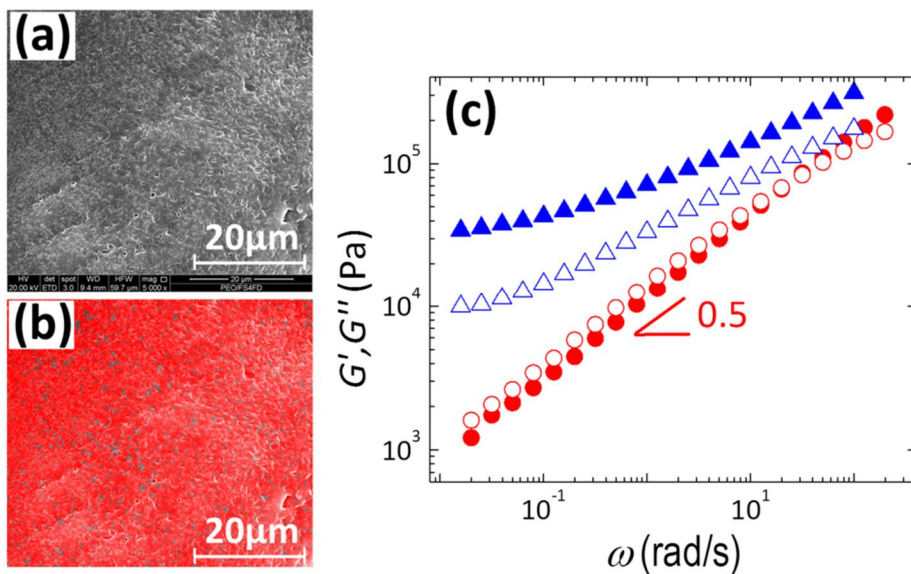


Figure 4. (a) SEM micrograph of the FD sample at $\phi \approx 4\%$; the same picture is shown in (b) with the X-ray map of the Silicon superimposed on it. (c) G' (full symbols) and G'' (empty symbols) of the FD (triangles) and MC (circles) samples at $\phi \approx 4\%$.

The degree of dispersion of the filler is clearly higher than that observed for the MC sample at the same composition. This has a remarkable impact on the melt state rheological behavior. The comparison between the linear viscoelastic moduli of the MC and FD composites at $\phi \approx 4\%$ is shown in Figure 4.c. The MC sample exhibits gel-like behavior whereas the FD sample has a predominantly elastic connotation typical of solid-

like materials, with G' displaying a weak ω -dependence and remaining higher than G'' in the whole investigated frequency range. The frequency dependence of the linear viscoelastic moduli for the FD samples at different ϕ is reported in Figure 5.

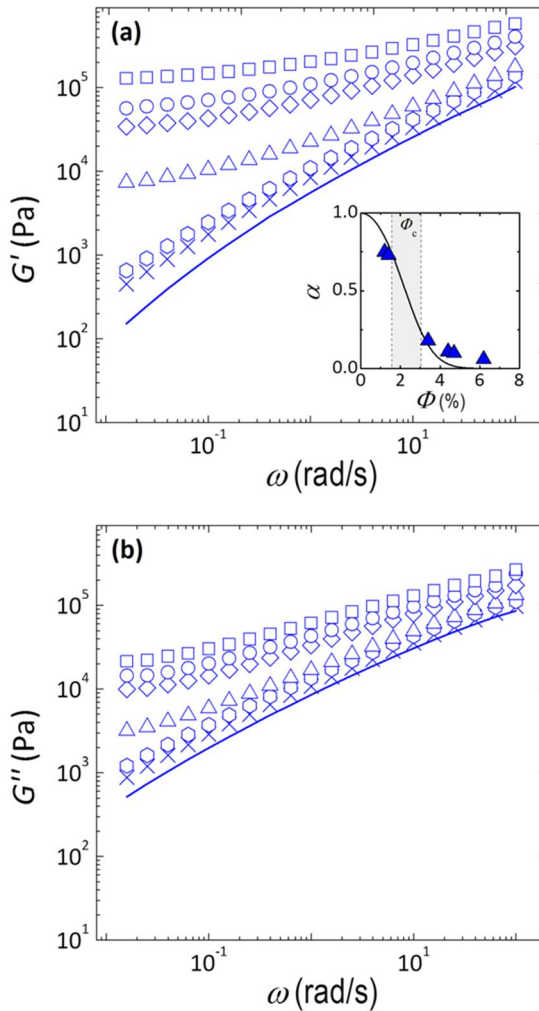


Figure 5. Frequency dependence of the linear elastic (a) and viscous (b) moduli of the neat PEO (solid line) and the FD samples at different filler content: from bottom to top, $\phi=1.2\%$, 1.4% , 3.4% , 4.4% , 4.7% and 6.2% . The inset in (a) shows the low frequency log-log slope of $G'(\phi)$ normalized to that of the pure polymer, $\alpha(\phi)$.

The dynamic response of these composites qualitatively resembles that of the MC ones. In the FD samples, however, the transition to a solid-like behavior occurs at lower filler content. This is clearly shown in the inset of Figure 5.a, where the dimensionless slope $\alpha(\phi)$ already falls down at $\phi\approx 3\%$. Such a result confirms that the percolation threshold for the FD composites is lower than that for the MC ones, the ϕ_c being very sensitive to the state of particle dispersion. Surprisingly, despite such morphological differences, the two series of samples at $\phi>\phi_c$ share the same melt state dynamics. This is shown in Figure 6.a, where the master curve of G' for the FD samples is superposed to that of the MC systems. The two curves lay on top of each other, suggesting that the stress-bearing mechanisms responsible for the gradual slowing down of the relaxation dynamics are the same. The main difference with respect to the MC systems emerged when scaling the data relies on the $B(\phi)$ values (Figure 6.b). The higher hydrodynamic disturbance noticed for the FD samples reflects the better dispersion of silica particles. Nevertheless, once such hydrodynamic effects have been properly

accounted for, the two families of samples only differ in terms of the size of the “building block elements” of the network.

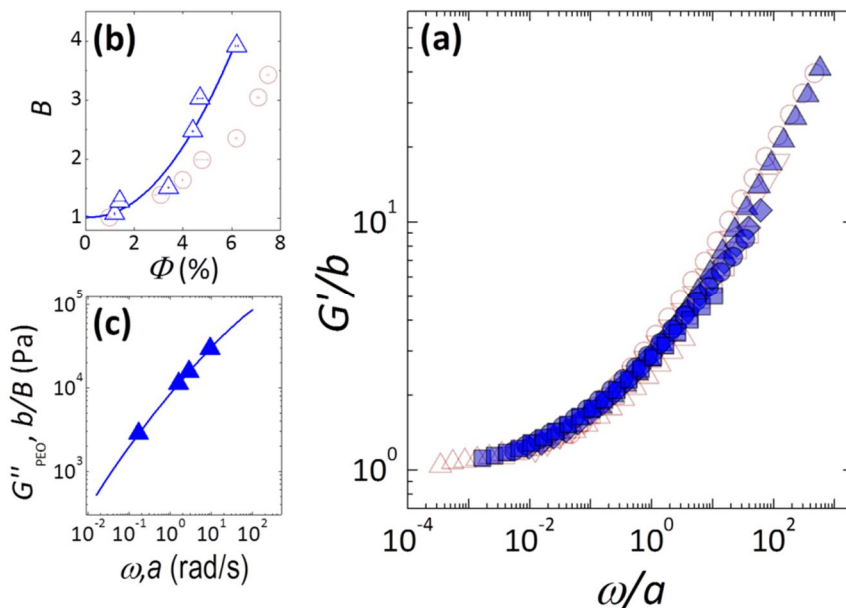


Figure 6. (a) Master curve of G' of the FD samples (triangles); the master curve for the MC samples (empty symbols) is also shown. (b) Amplification factors $B(\phi)$ of the FD (triangles) samples; the $B(\phi)$ of the MC samples (circles) are reported for comparison; the line is a guide for the eye. (c) Factors used to shift the G' curves of the FD samples; the points lie on the viscous modulus of the freeze-dried neat PEO.

3.3.4 Elasticity and structure of the PEO/SiO₂ composites above ϕ_c

To directly compare the stress bearing mechanisms of the network forming in the MC and FD systems, we analyze their ϕ dependent

elasticity, G'_0 . Percolation theories predict the network elasticity to grow with ϕ as:

$$G'_0 \sim (\phi - \phi_c)^\nu \quad (1)$$

where the exponent ν is related to the stress-bearing mechanism²⁵.

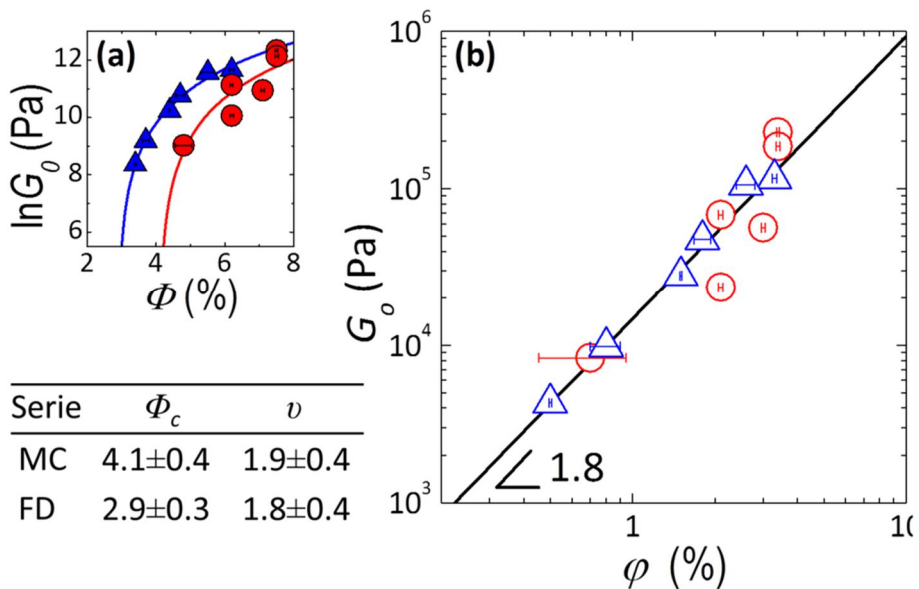


Figure 7. (a) ϕ -dependent elasticity of the networks forming in the MC (circles) and FD (triangles) samples; lines are the fit of Eq. 1 to the experimental points. The fitting parameters ϕ_c and ν are summarized in the table. (b) Universal scaling with ϕ of the network elasticity for the studied samples.

The $G'_0(\phi)$ of the MC and FD samples correspond to the vertical shift factors b used to scale the G' curves for the building of the master curves of Figure 3 and 6. By independently fitting Equation (1) to each dataset we get ϕ_c and ν for the two families of samples (Figure 7.a). The values of the percolation thresholds are in line with those inferred by analyzing the dimensionless slopes $\alpha(\phi)$, confirming the better degree of filler dispersion in the FD samples. When plotted against the rescaled volume fraction $\varphi = \phi - \phi_c$, however, the elasticity of the two systems collapse onto the same line, $G'_0 \sim \varphi^\nu$, with $\nu \approx 1.8$. This supports our previous conclusion about the common nature of the stress transfer mechanism, which seems to be dictated by the polymer-particle pair rather than by the degree of filler dispersion. The value of the critical exponent suggests that the networks have the structural characteristics of polymer bridged colloidal gels forming in attractive polymer-particle mixtures, as delineated by Surve et al.²⁶. The results of their simulations indicate that the overall structural features of such kinds of gels resemble those of random percolation models with the elasticity exponent $\nu \approx 1.88$. The enhanced elastic response and solid-like behavior exhibited by the studied PEO/SiO₂ nanocomposites above ϕ_c are therefore consistent with a networking mechanism based on polymer-mediated interactions between silica aggregates. This is schematically sketched in Figure 8, where the different degrees of dispersion between the FD and MC samples are conveniently highlighted.

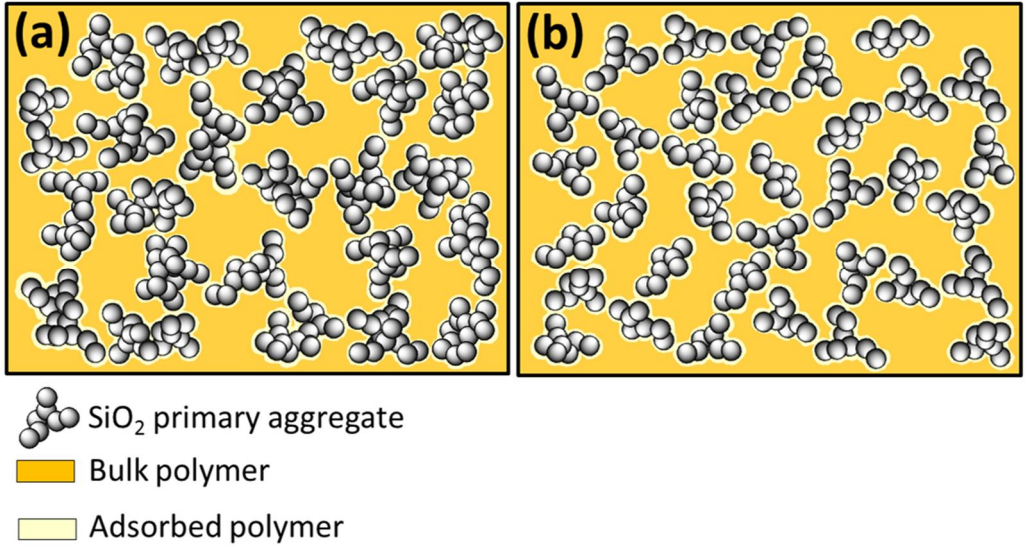


Figure 8. Schematic representation of the structure of the MC (a) and FD (b) samples above ϕ_c as emerged from morphological and linear viscoelastic analyses. The filler networks are mediated by a thin shell of adsorbed polymer surrounding the SiO_2 aggregates.

3.4 Conclusions

We have studied the structure and linear viscoelasticity of PEO/ SiO_2 composites as function of particle volume fraction. The samples have been prepared by two different compounding procedures to highlight the effect of the initial state of filler dispersion on their macroscopic elastic properties. Both families of composites have qualitatively similar

viscoelastic features. In particular, a critical volume fraction can be identified above which a clear solid-like connotation emerges. Improving the filler dispersion shifts the liquid- to solid-like transition at lower filler content. Irrespective of the initial state of dispersion, however, the solid connotation arises from the presence of stress-bearing networks, whose elasticity exhibits a power-law dependence on particle volume fraction. Above the percolation threshold the elastic response of both series of composites can be described assuming the independence of the responses of two main populations of dynamical species: a fraction of bulk polymer, whose relaxation modes are not affected by the presence of the filler, and a much slower superstructure, consisting of particles covered with a shell of adsorbed polymer. This allows for the separation of the contributions of the two families, validated through the scaling of the elasticity of samples at different volume fractions on a single master curve. The universal linear viscoelastic response of the studied composites thus becomes evident: irrespective of the compounding procedure, above the percolation threshold the building blocks of the network interact through a polymer-mediated mechanism. The analysis of the critical exponents for the scaling of the elasticity with volume fraction supports such conclusion.

Chapter 4

Role of Polymer–Particle interactions on the Dynamics of Polymer Nanocomposites

Glass Transition and Reinforcement Mechanism in PMA/SiO₂ Mixtures

4.1 Introduction

A polymer nanocomposite is a polymer matrix with a reinforcing phase consisting of particles with one dimension in the nanosized regime. In the past decade, extensive research has focused on polymer nanocomposites in hopes of exploiting the unique properties of materials in the nanosized regime. A general conclusion has been drawn that nanocomposites show much improved mechanical properties over similar microsized systems because of their small size. A desirable result of embedding nanoparticles into a polymer matrix is the enhanced

bonding between the polymer matrix and filler, resulting from the nanoparticles' high interfacial energy. Classical composite theory predicts that improved bonding between the polymer matrix and the reinforcing phase leads to improved mechanical properties. Despite these predictions, however, mechanical tests of nanocomposites have shown controversial results. No clear conclusions have been made regarding trends in the mechanical properties of polymer nanocomposites, as current polymer models have not been able to consistently predict the properties of nanocomposites. Polymer composite theories in the past have relied on the idea that the modulus of a composite is a function of the mismatch of properties of constituents, volume fraction, shape and arrangement of inclusions, and matrix-inclusion interface. These theories, therefore, predict that the effect on the composite system is independent of the size of the inclusion. Recent theories have included the size of the filler particulate to predict the properties of composites. An area of polymer composite structure that has always garnered attention is the region near the interface of the polymer matrix and the filler. Despite the large variety of polymer composite systems, a common thread among all the systems is the existence of a phase border between the matrix and filler and the formation of an interphase layer between them. The interphase layer is believed to extend well beyond the adsorption layer of the matrix chains bound to the filler surface. The structure of the interphase is

different than either the filler or matrix phases, and it varies depending on the distance from the bound surface. Because of the structural differences, the properties of the polymer at the interface can differ dramatically from the bulk polymer. The interphase structure and properties are important to the overall mechanical properties of the composite because its distinct properties control the load transfer between matrix and filler. The concept of interphase is not unique to nanocomposites, but because of the large surface area of nanoparticles, the interphase can easily become the dominating factor in developing the properties of nanocomposites. A 1 nm-thick interface surrounding microparticles in a composite represents as little as 0.3% of the total composite volume. However, a 1 nm-thick interface layer on nanoparticles can reach 30% of the total volume. The interphase has a characteristic structure consisting of flexible polymer chains, typically in sequences of adsorbed segments (point contacts, i.e., anchors, or trains) and unadsorbed segments, such as loops and tails, which in turn are entangled with other chains in their proximity and which are not necessarily bound to the surface. Interphase thickness for a specific particle-polymer system is not a constant size because the interphase has no well-defined border with the bulk polymer. The effective value of the thickness depends on chain flexibility, the energy of adsorption, and the extent of chain entanglements, which are determined by the surface energies of the polymer and the nanoparticles. Because of

conformational limitations brought by particles in addition to other restrictions on chain conformation, only a relatively small number of segments within a chain are directly bound to the surface. If all areas of the surface are capable of adsorption, then polymer segments, for a reasonably flexible polymer -chain, are readily adsorbed on the surface, resulting in short loops and a flat (i.e., dense) layer close to the surface. If the chain segments have weak interaction with the surface or if the chain is rigid, the loops and tails extend farther into the matrix and form a region of lower density. Therefore, the strength of the interaction of a polymer molecule with the surface of the nanoparticles controls both the polymer molecular conformations at the surface and the entanglement distribution in a larger region surrounding the nanoparticle. Hence, a higher degree of entanglements will result in a larger number of polymer chains that are associated with a given nanoparticle, of which only a fraction are actually anchored to the surface.

In this chapter we study the dynamical properties of polymer nanocomposite systems based on Poly(methylacrylate) and silica (SiO_2) and investigated the role of polymer-particle interactions as well as particle size on their behavior. The nanoparticles were dispersed in PMA matrices through a solvent mediated process. Colloidal (15 nm) spherical silica nanoparticles and pyrogenic fumed silica (100 nm) were chosen as fillers on the basis of availability and size distribution and due

to the existence of results from literature for comparison. PMA was chosen as the matrix material on the basis of its potential interactions with such particles. Previous studies have shown that PMA adsorbs strongly to metal oxide nanoparticles through coordination of the carbonyl functional group to the silanols surface sites. High molecular weight polymers with $80000\text{g/mol} < M_n < 96000\text{ g/mol}$ and $M_w/M_n < 1.2$ were chosen to maximize chain flexibility, which facilitates chain adherence to a nanoparticle surface.

4.2 Experimentatl

4.2.1 Raw materials

All materials were used as-received. 2-butanone (MEK, 99%), was purchased from Acros Organics (Geel, Belgium). Silica (SiO_2) nanoparticles suspended in 2-butanone (Organosilicasol MEK-ST) were supplied by Nissan Chemical America (Houston, TX). The silica nanoparticles were characterized by the manufacturer using electron microscopy as polydisperse spheres with diameters in the range 10-15 nm.

Poly(methyl acrylate) (PMA, $M_n = 80000\text{Kg/mol}$ and $M_n = 96000\text{ Kg/mol}$, $M_n/M_w = 1.2$) was synthesized via atomtransfer radical polymerization

(ATRP). The synthesis procedure was similar to that employed by Matyjaszewski at al. 132 mg of CuBr catalyst was placed in a 300 mL flask. 100 mL of methyl acrylate was passed through a basic alumina column and into the flask. 190 μ L of PMDETA (pentamethyldiethylenetriamine) was added to the solution, which was then sealed with a rubber septum. To remove oxygen, the flask was then purged with nitrogen gas for 5 min followed by bubbling nitrogen gas through the solution for 25 min. 120 μ L of initiator (ethyl α -bromoisobutyrate) was injected into the flask. The homogeneous solution was immersed in an oil bath held at 100 °C with constant stirring at 400 rpm via a magnetic stir bar for 7h. After cooling in an ice water bath, about 150 mL of tetrahydrofuran was added. The solution was then passed through a neutral alumina column to remove the catalyst and precipitated into hexanes, filtered, and dried under vacuum. Molecular weight characterization was done by gel permeation chromatography using PMMA standards for calibration.

4.2.2 Nanocomposites preparation.

PNC were precipitated in hexane from semi-dilute solutions of PMA in MEK with added silica nanoparticles. After evaporation of the solvent the samples were annealed at 80°C for 24h. To achieve good mixing during preparation, we employed a 750 W probe ultrasonicator fitted with a tapered tip.

4.2.3 Characterization

Dynamic-mechanical analyses (DMA) were carried out using a Tritec 2000 DMA (Triton technology, UK). The dynamic moduli were measured as a function of temperature in single cantilever bending mode at a frequency of 1 Hz and total displacement of 0.03 mm, which is small enough to be in the linear regime. The sample bars were heated at 2°C / min from about -50°C to either 0°C or 80°C depending on their composition. Rheological analyses were performed using a strain-controlled rotational rheometer (TA Instruments mod. ARES) in parallel plate geometry (diameter 25 mm). Measurements were carried out at different temperatures ($35^{\circ}\text{C} < T < 120^{\circ}\text{C}$) in a dry nitrogen atmosphere. Viscoelastic analyses were performed in the linear regime, which was established for each sample through preliminary strain-sweep tests. Due to a marked sensitivity of the rheological properties to the filler content, thermogravimetric analyses (TGA) were performed on the samples recovered at the end of rheological tests. The weight fractions deduced from TGA were converted into volume fractions (ϕ) using the bulk densities of the components. The morphology of the filled samples on nanoscale was inspected through transmission electron microscopy (TEM) using a Philips EM 208 TEM with 100 keV accelerating voltage. The specimens were in the form of thin slices (thickness ≈ 150 nm) cryosectioned using a diamond knife.

4.3 Results and discussion

4.3.1 Structure and dynamics PMA/Colloidal Silica mixtures

Glass transition

During the glass transition, the polymer chains gain mobility and thus dissipate a great amount of energy through viscous movement. This is shown in the $\tan\delta$ peak in a DMA test. The temperature at the maximum value of $\tan\delta$ peak has been often regarded to be the value of T_g . The height depression in the $\tan\delta$ peak indicates that there is a reduction in the amount of mobile polymer chains during the glass transition and hence can be used to estimate the amount of constrained chains. Therefore DMA can provide indirect but useful evidence of structural attributes.

The dynamic mechanical moduli of PMA filled with spherical silica nanoparticles show no significant changes in the glassy or rubbery state with respect to the neat polymer. At the α -transition, a substantial drop in E' occurs while E'' exhibits a peak, which is indicative of viscous damping (data not shown). Figure 1 shows the $\tan\delta$ (E''/E') curves for the neat polymer and the composites at different concentrations.

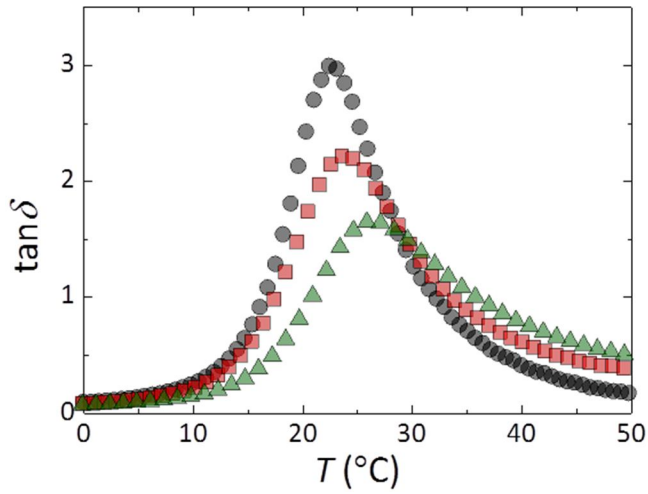


Figure 1. $\tan\delta$ spectra for the neat PMA (circles) and the PMA-based SiO_2 nanocomposites at $\phi=7.7\%$, (squares) and $\phi=13.2\%$ (triangles).

The nanocomposites display a shift in the $\tan\delta$ peak toward higher temperatures compared with the pure polymer. Further, the addition of nanofillers results in a decrease in the magnitude of the $\tan\delta$ peak along with an increase in its width. Similarly, the change in heat capacity of the materials associated with the glass transition shifts to higher temperatures upon particle addition, but the magnitude and breadth of the change remain unaltered. The change in T_g from that of pure PMA for the PMA/ SiO_2 PNCs, as measured by both DSC and DMA, is shown in Figure 2.

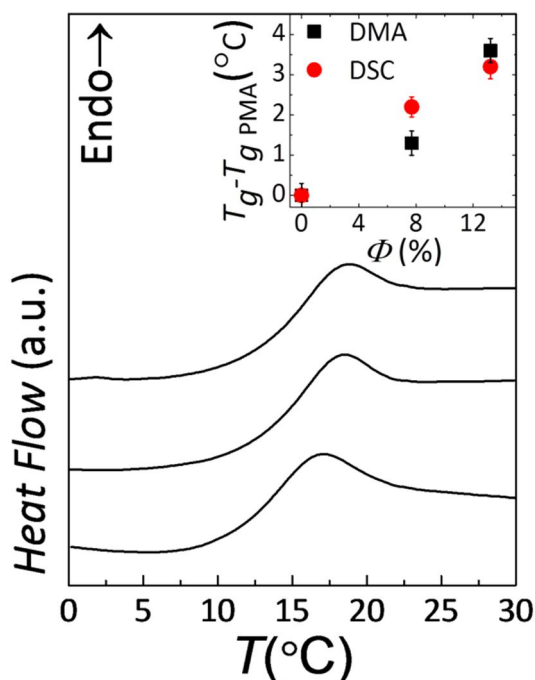


Figure 2. Representative DSC curves in the glass-transition region for the neat PMA and the PMA-based SiO₂ nanocomposites at $\phi=7.7\%$, and $\phi=13.2\%$ (from bottom to top). (Inset) Change in T_g from that of pure PMA for the as measured by both DSC and DMA

The DSC T_g was determined in the following manner: (1) straight lines were fit to the heat flow vs temperature curves before, during, and after the glass transition; (2) the points of intersection were taken as the onset and end point of the transition; and (3) the T_g was taken as one-half the change in heat capacity between the onset and end point of the transition. The DMA T_g was identified as the peak position of

$\tan\delta$ plotted as a function of temperature. It is clear from Figure 2 that the T_g of the material slightly increases with the addition of spherical silica nanoparticles.

Linear Viscoelasticity

Rheological measurements were conducted to determine the effect of nanosized spherical SiO_2 particles on the dynamics and topology of the polymer melt. Master curves of the storage (G') and loss (G'') moduli at a reference temperature, $T_0=90^\circ\text{C}$, are shown in Figure 3 as a function of the reduced frequency.

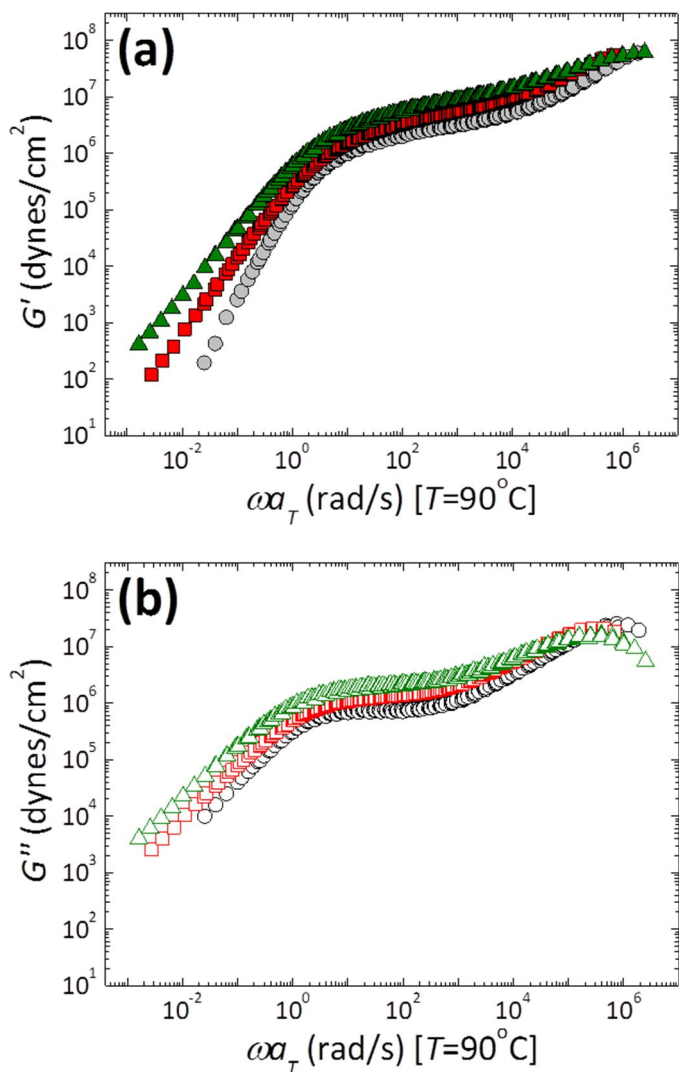


Figure 2. Time temperature superposed mastercurves of the linear elastic G' (a) and viscous G'' (b) moduli of the neat PMA (circles) and the PMA/SiO₂ nanocomposites at $\phi=7.7\%$, (squares) and $\phi=13.2\%$ (triangles).

The unfilled PMA has the characteristic viscoelastic response of a linear homopolymer displaying well defined transition and entanglement regions along with a low-frequency crossover, below which it relaxes in a liquid-like fashion ($G' \sim \omega^1$ and $G'' \sim \omega^2$). Even at relatively high loadings, the addition of silica does not significantly change the viscoelastic behavior of the polymer. The same features, including the liquid-like relaxation at low frequencies, are observed for the two nanocomposites. Corroboration of the observed linear viscoelastic response is obtained from the stress-relaxation behavior of the homopolymer and the composites shown in Figure 4. One of the notable features in the stress-relaxation data is the equivalence between the linear stress relaxation measurements and the calculated stress-relaxation data based on the linear dynamic oscillatory shear response and a two-point collocation methodology developed by Ferry and co-workers. Such method relates the linear stress relaxation $G(t)$ to the corresponding dynamic moduli by

$$G(t) = G'(\omega) - 0.40G''(0.40\omega) + 0.014G''(10\omega) \Big|_{\omega=1/t} \quad (2)$$

and contains no adjustable parameters. The agreement between the measured linear stress relaxation modulus and those calculated from linear dynamic data is noteworthy and suggests that both the oscillatory and stress-relaxation measurements are indeed representative linear viscoelastic data.

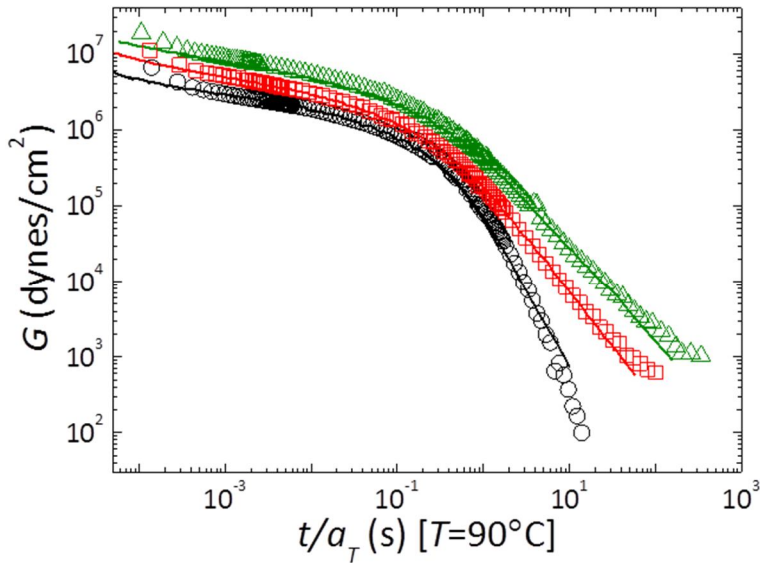


Figure 4. Time-temperature superposed relaxation data after instantaneous step shear deformation for the neat PMA (circles) and the PMA/SiO₂ nanocomposites at $\phi=7.7\%$, (squares) and $\phi=13.2\%$ (triangles). The lines are the predictions based on the application of eq. 1 and using the data obtained from linear dynamic viscoelastic measurements on the same samples.

Essentially, the nanofiller determines a shift of the moduli to higher magnitudes and lower frequencies. The change in the magnitude of the storage modulus with SiO₂ content is evaluated in terms of the plateau modulus G_N^0 , whereas the frequency shift in the moduli is evaluated in terms of the longest relaxation time of the polymer, τ_R , which is the reptation time for our entangled PMA. An estimate of G_N^0 for the materials is obtained from the value of the elastic shear modulus at the

point of maximum elasticity (i.e when $\tan\delta$) reaches the minimum value) and is depicted as a function of silica content in Figure 5.a. The longest relaxation time of the polymer is estimated as the reciprocal of the crossover frequency of storage and loss moduli and is plotted against ϕ in Figure 5.b. We use the two parameters G_N^0 and τ_R to rescale the modulus and frequency axes of the data in Figure 2.a. to further highlight the changes in the relaxation spectra. The rescaled data are reported in Figure 5.c.

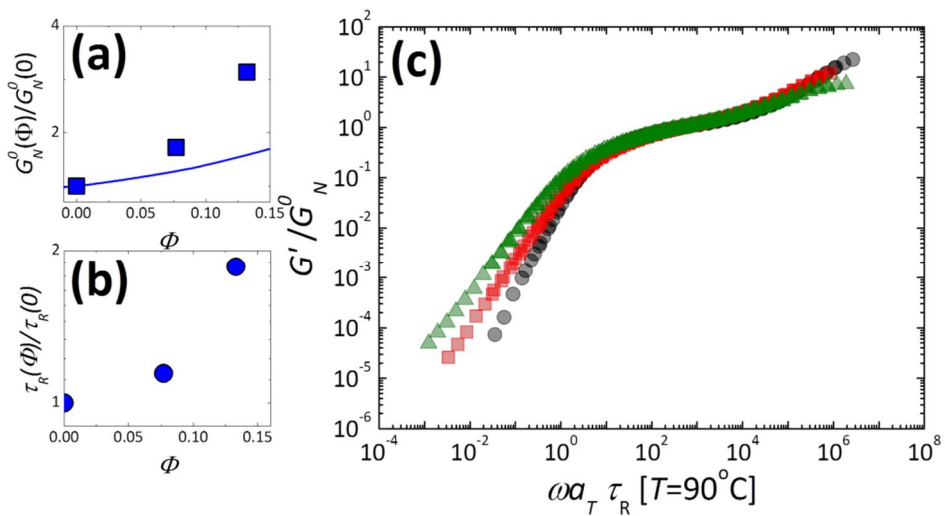


Figure 5. (a) Ratio of the plateau moduli of the PNCs to that of pure PMA as a function of SiO_2 volume fraction. The Guth-Smallwood relation (line) is plotted along with the data for comparison. (b) Ratio of the longest relaxation time for the PNCs to that of pure PMA as a function of SiO_2 loading. (c) Dynamic shear moduli rescaled as described in the text.

The shift factors, a_T , necessary to build the master curves of the viscoelastic moduli for the PMA matrix and each PNC are plotted as a function of temperature in Figure 6. The data from all samples can be described by the Williams-Landel-Ferry (WLF) relation at the reference temperature $T_0=90^\circ$.

$$\log(a_T) = \frac{-C_1(T-T_0)}{C_2+T-T_0}$$

The ability to describe all data in Figure 7 by a single fit of eq 3 (with $C_1=5.9-6.3$ and $C_2=127-140$) suggests that the temperature dependence of the relaxation dynamics is similar in the composites and in the unfilled polymer. The positive deviations from the shift factors of the neat PMA observed for the composites only at low temperatures are consistent with the existence of fraction of chains whose relaxation is governed by a higher monomeric friction coefficient. Such constrained population is responsible for the increase in the dynamic T_g discussed above. When plotted against $T-T_g$ the data collapse onto a single curve as shown in the inset of Figure 6.

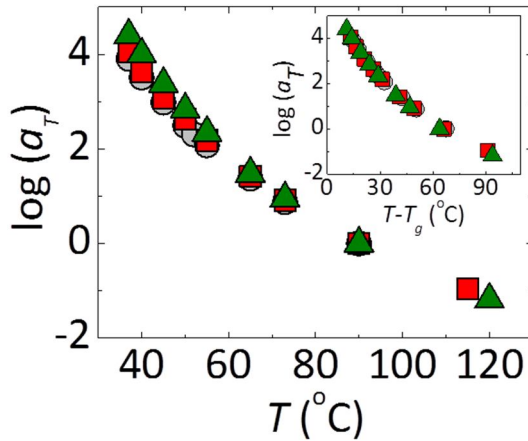


Figure 5. Temperature dependence of the frequency shift factors for the neat PMA (circles) and the PMA/SiO₂ nanocomposites at $\phi=7.7\%$, (squares) and $\phi=13.2\%$ (triangles). The same data are recast in the inset as a function of $T-T_g$.

4.3.2 Dispersion morphology

Cross-sectional transmission electron microscopy (TEM) images of the PNCs (Figure 8) at different magnifications reveal that the filler exists as individual particles ($d \approx 20\text{nm}$) as well as in the form of nanoscopic agglomerates with diameters on the order of 50nm. These observations aggregates at these low concentrations can still be described as nanoparticles.

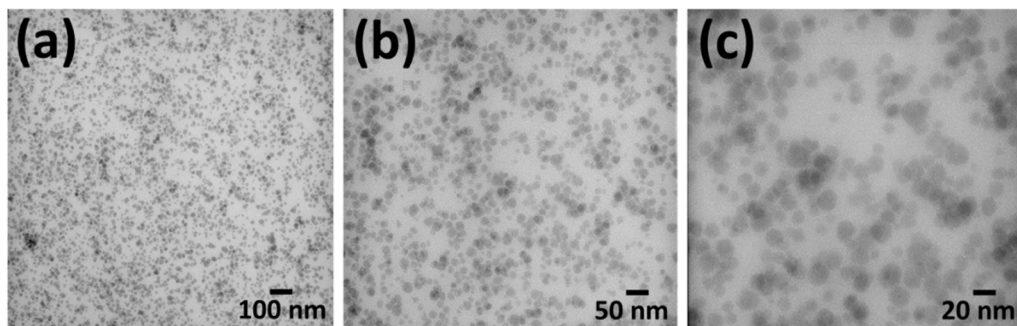


Figure 7. TEM morphology of a PMA/SiO₂ nanocomposite at $\phi=7.7\%$.

4.4 Origin of the dynamic behaviour

As described in the Introduction, the property enhancements exhibited by PNCs can result from two effects: (1) a “filler” effect that can be completely described by the volume fraction of particles and has been well characterized through studies of conventional composites and/or (2) changes in the polymer matrix properties due to specific interactions between the polymer chain segments and the nanoparticles. While the latter is relevant in many systems, the specific mechanisms behind the influences are often not fully understood. Simulations suggest that the presence of nanoparticles change the local monomer packing and that such changes in structure can contribute to the observed property enhancements. For instance, a decrease in fractional free volume associated with increased monomer packing density, due to the influence of nanoparticles, could account for the increase in T_g exhibited

by our PMA/SiO₂ systems, assuming the glass transition is an iso-free volume process. The increase in T_g could, in turn, account for the slowing-down of the melt dynamics. Another scenario might be that an increase in polymer entanglement density arises from increased monomer packing density or direct polymer-particle contacts. The resulting decrease in the number of monomers between entanglements, N_e , could account for increases in the entanglement plateau modulus and chain relaxation time exhibited by the PMA/SiO₂. However, our experimental observations suggest that the increase in G_N^0 with silica concentration is also associated with the “filler” effect. In addition, we illustrate that the perturbing influence of the nanoparticles on the polymer matrix does not derive from polymer chain confinement or polymer bridging between particles²⁷. Instead, we argue that the increases in τ_R and T_g reflect the subtle influence of transient interactions between the silica surfaces and the PMA chain segments.

4.4.1 Free Volume and Polymer Entanglement Density.

As just described, changes in system free volume and/or polymer entanglement density²⁸, due to an influence of nanoparticles on polymer packing, could be responsible for changes in T_g , τ_R , and G_N^0 in PNCs. For instance, in PMMA-POSS PNCs, a WLF analysis enables a rationalization of the changes in system T_g in terms of changes in free volume with POSS concentration. The rheological measurements of the

PMA/SiO₂ PNCs, however, fail to resolve any such changes in structure. The WLF constants are almost independent of silica concentration in these materials, which suggests that free volume changes cannot explain the trends exhibited in T_g . However, an analysis of the breadth of the plateau region of the rheological data reveals that the PMA entanglement density increases with concentration. A change in N_e results in a change in the breadth of the plateau region. The normalized data in Figure 6 illustrates such changes; the data for the homopolymer and all PNCs does not superpose over the entire frequency range. Deviations are observed in the regions of the spectrum which extend beyond the plateau region at both high and low frequencies. The changes in the breadth of the plateau region suggests that the observed changes in G_N^0 might be the result of changes in the entanglement density.

4.4.2 The “Filler” Effect.

We now examine the increase in melt plateau modulus with SiO₂ concentration using a continuum theory which describes the effect of hard, noninteracting, spherical fillers on the moduli of polymers. The theory relates the modulus of the composite, to that of the polymer by a filler volume fraction dependent term.

$$G_N^0(\phi) = G_N^0(0)[1 + 2.5\phi + 14.1\phi^2]$$

While such equation, often referred to as the Guth-Smallwood equation, under predicts the compositional dependence of the modulus depicted in Figure 5. The discrepancy can be accounted for by a number of factors including the anisotropy of the nanoscopic aggregates (emerging from TEM) and the presence of occluded rubber. Both effects tend to increase the magnitude of G_N^0 beyond the theoretical predictions.

4.4.3 Factors of Influence on PMMA Matrix Properties.

Our results show that SiO_2 perturbs the polymer matrix in such a manner as to increase the T_g and polymer chain relaxation time²⁹. The confinement of chains between filler particles, polymer bridging between particles, and polymer-particle interfacial interactions may all contribute toward the influence that nanoparticles have on the properties of polymers. We now examine the relative role these factors play in shaping the properties exhibited by the PMA/ SiO_2 . Chain confinement effects are expected to be significant when interparticle distances, h , become smaller than the size of the polymer, $2R_g$. Assuming that the particles are individually dispersed, an estimate of the interparticle distance, h , using the particle diameter (20nm) and the volume fraction suggests that the polymer chains are not experiencing confinement, especially if aggregation is taken into account. Therefore, confinement of the polymer chains between particles does not contribute to the observed changes in T_g and chain

dynamics. Polymer chain bridging between particles also requires that the size of the polymer chain exceed the interparticle distances. However, we have already established that $h > 2Rg$ in the ourmixtures, so any mechanism based solely on particle bridging would not be significant. Moreover, the lack of formation of a percolated filler network mediated by polymer chains, associated with polymer bridging between particles, is also evident from the melt dynamic shear moduli in the low frequencies regime. Such a network restrains long-range motions of polymer chains; the liquid-like terminal behavior associated with homopolymers at long time scales transitions to solidlike behavior. However, the PMA/SiO₂ materials exhibit homopolymer-like terminal flow behavior, and only a slowing down occurs. This behavior is in contrast to that of a percolated network, where influence would primarily result in a solid-like behavior. Hence, both interparticle distances that exceed polymer chain size and the terminal flow behavior of the materials indicate that polymer bridging between particles is not the contributing influence to the changes in T_g and chain dynamics observed for our PNCs. The absence of polymer chain confinement and polymer bridging between particles leaves interfacial interactions to account for the observed changes in PMMA matrix properties³⁰.

4.4.4 Role of Interfacial Interactions.

There is reasonable insight into ways that interfacial interactions influence the properties of polymers, particularly from measurements of the glass transition temperature of thin polymer films and of PNCs³¹. In PNCs, particles are generally described to influence the glass transition of the material in one of two manners. The first is a relatively long-ranged gradient in T_g , extending tens of nanometers from the interface, that influences the average T_g of the material. The second is a more localized effect denoted by marked changes in polymer dynamics at direct interfacial contact with the particles, i.e., "bound" polymer³², while, at the same time, homopolymer-like dynamics are exhibited by chains away from the particle surface. For the PMA/SiO₂ system a long-ranged gradient in the polymer T_g within the interfacial region produces a broader distribution of polymer relaxation times compared to the homopolymer and hence broaden the width of the glass transition peak for the PNCs relative to the homopolymer. The marked change in dynamics at interfacial contact results in the shift the relaxation of a fraction of polymer segments outside the spectrum of the homopolymer peak and hence reduce the peak of the PNCs.

To further support this claim we show the melt elasticity of PMA filled with fumed silica nanoparticles at different concentrations (Figure 8). Here the increased interfacial interactions, due to hydrogen bonding

between the carbonyls of PMA and the silanols of silica, contributes to the reinforcement and eventually result in the formation of a percolated polymer-filler network^{33,34}.

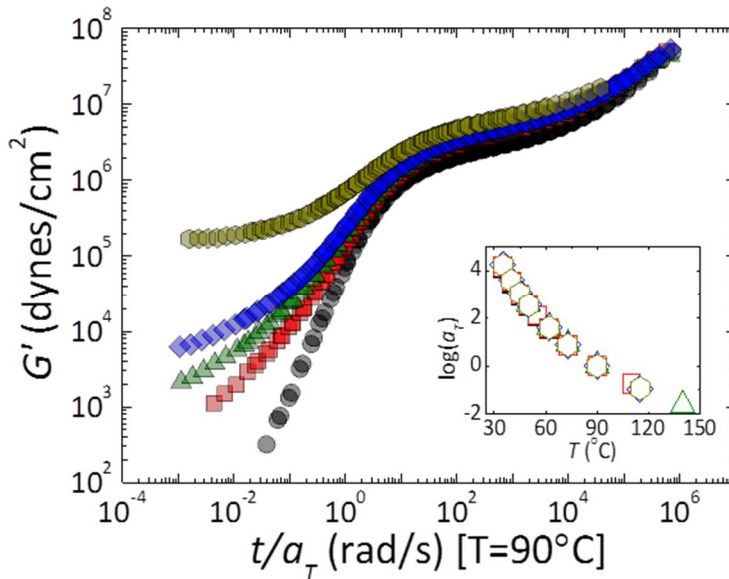


Figure 2. Time temperature superposed mastercurves of the linear elastic G' (a) modulus of the neat PMA (circles) and the PMA/ fumed SiO_2 nanocomposites at $\phi=2.4\%$, (squares), $\phi=4.1\%$ (triangles), $\phi=5.1\%$ (diamonds) and $\phi=6.2\%$. The shift factors as a function of temperature are reported in the inset.

REFERENCES

- 1) Galindo-Rosales, F. J.; Moldenaers, P.; Vermant, J. *Macromolecular Materials and Engineering*, 296, 331-340.
- 2) Jancar, J.; Douglas, J. F.; Starr, F. W.; Kumar, S. K.; Cassagnau, P.; Lesser, A. J.; Sternstein, S. S.; Buehler, M. J. *Polymer* 2010, 51, 3321-3343.
- 3) Acierno, D.; Filippone, G.; Romeo, G.; Russo, P. *Macromolecular Symposia* 2007, 247, 59-66.
- 4) Jancar, J.; Recman, L. *Polymer* 2010, 51, 3826-3828.
- 5) Romeo, G.; Filippone, G.; Russo, P.; Acierno, D. *Polymer Bulletin* 2009, 63, 883-895.
- 6) Ozmusul, M. S.; Picu, C. R.; Sternstein, S. S.; Kumar, S. K. *Macromolecules* 2005, 38, 4495-4500.
- 7) Saint-Michel, F.; Pignon, F. d. r.; Magnin, A. *Journal of Colloid and Interface Science* 2003, 267, 314-319.
- 8) Zhang, Q.; Archer, L. A. *Langmuir* 2002, 18, 10435-10442.
- 9) Zhu, Z.; Thompson, T.; Wang, S.-Q.; von Meerwall, E. D.; Halasa, A. *Macromolecules* 2005, 38, 8816-8824.
- 10) Acierno, D.; Filippone, G.; Romeo, G.; Russo, P. *Macromolecular Materials and Engineering* 2007, 292, 347-353.
- 11) Galgali, G.; Ramesh, C.; Lele, A. *Macromolecules* 2001, 34, 852-858.
- 12) Inoubli, R.; Dagregou, S.; Lapp, A.; Billon, L.; Peyrelasse, J. *Langmuir* 2006, 22, 6683-6689.
- 13) Ren, J.; Silva, A. S.; Krishnamoorti, R. *Macromolecules* 2000, 33, 3739-3746.
- 14) Filippone, G.; Romeo, G.; Acierno, D. *Langmuir* 2009, 26, 2714-2720.
- 15) Romeo, G.; Filippone, G.; Fernández-Nieves, A.; Russo, P.; Acierno, D. *Rheologica Acta* 2008, 47, 989-997.
- 16) Engin, B. *Polymer* 2011, 52, 5118-5126.
- 17) Raghavan, S. R.; Walls, H. J.; Khan, S. A. *Langmuir* 2000, 16, 7920-7930.
- 18) Voronin, E. F.; Gun'ko, V. M.; Guzenko, N. V.; Pakhlov, E. M.; Nosach, L. V.; Leboda, R.; Skubiszewska-ZiÅ™ba, J.; Malysheva, M. L.; Borysenko, M. V.; Chuiko, A. A. *Journal of Colloid and Interface Science* 2004, 279, 326-340.
- 19) Kammler, H. K.; Beaucage, G.; Mueller, R.; Pratsinis, S. E. *Langmuir* 2004, 20, 1915-1921.

- 20) Mueller, R.; Kammler, H. K.; Wegner, K.; Pratsinis, S. E. *Langmuir* 2002, 19, 160-165.
- 21) Gleissle, W.; Hochstein, B. *Journal of Rheology* 2003, 47, 897-910.
- 22) Winter, H.; Mours, M.; Springer Berlin / Heidelberg, 1997, p 165-234.
- 23) Madathingal, R. R.; Wunder, S. L. *Macromolecules* 2011, 44, 2873-2882.
- 24) Sternstein, S. S.; Zhu, A.-J. *Macromolecules* 2002, 35, 7262-7273.
- 25) Stauffer, D. A., A. *Introduction to Percolation Theory*: London, 1992.
- 26) Surve, M.; Pryamitsyn, V.; Ganesan, V. *Physical Review Letters* 2006, 96, 177805.
- 27) Robertson, C. G.; Lin, C. J.; Rackaitis, M.; Roland, C. M. *Macromolecules* 2008, 41, 2727-2731.
- 28) Heinrich, G.; Vilgis, T. A. *Macromolecules* 1993, 26, 1109-1119.
- 29) Jouault, N.; Vallat, P.; Dalmas, F.; Said, S. r.; Jestin, J.; Bouel , F. o. *Macromolecules* 2009, 42, 2031-2040.
- 30) Bailly, M.; Kontopoulou, M.; El Mabrouk, K. *Polymer*, 51, 5506-5515.
- 31) Mortezaei, M.; Famili, M. H. N.; Kokabi, M. *Composites Science and Technology*, 71, 1039-1045.
- 32) Frohlich, J.; Niedermeier, W.; Luginsland, H. D. *Composites Part A: Applied Science and Manufacturing* 2005, 36, 449-460.
- 33) Ph, C. *Polymer* 2008, 49, 2183-2196.
- 34) Yurekli, K.; Krishnamoorti, R.; Tse, M. F.; McElrath, K. O.; Tsou, A. H.; Wang, H. C. *Journal of Polymer Science Part B: Polymer Physics* 2001, 39, 256-275.